Shkar Shaho

Finite-element modelling of the newborn middle ear at two different ages

Master Thesis

Submitted to the Faculty of Medicine of the
Eberhard Karls Universität Tübingen
In partial fulfillment of the requirements of the degree of Master of Science

In collaboration with the
Auditory Mechanics Laboratory, McGill University Montréal, Canada

Supervision

Prof. Dr. Tilman E. Schäffer
Prof. Dr. W. Robert J. Funnell

February 2020

Acknowledgements

This thesis would not have been possible without the support of many people. First and foremost, I offer my sincerest gratitude to my supervisor Dr. W. Robert J. Funnell at the McGill University for giving me the opportunity to conduct my research at the Auditory Mechanics Lab. His professional and valuable advice, his pioneering experience, and the patience during my thesis revision made this work possible.

Special thanks go also to Dr. Schäffer for his support and his willingness to supervise.

Thanks a lot, to the Auditory Mechanics Lab team for the great helpfulness and pleasant cooperation. A special thanks to Hamid Motallebzadeh for his valuable insights and his great support.

Last but not least, I would like to thank my beloved family who always supported and encouraged me.

Tübingen, February 2020 Shkar Shaho

Abstract

Hearing impairment is one of the most common birth defects and early identification is crucial for appropriate speech development. Unfortunately, current screening tools lack specificity and produce large numbers of false positives. Therefore, newborn middle-ear mechanics needs to be better understood in order to improve screening tools and thus improve the identification of conductive hearing loss and conditions like otitis media.

A finite-element model of the 1-day-old middle ear was generated and its response to a static pressure of 10 Pa was compared to an existing model of a 22-day-old middle ear in terms of displacement magnitudes and spatial patterns. Appropriate values for the material properties were taken from literature reviews and previous finite-element models. Furthermore, different shapes of the tympanic membrane were generated for the 1-day-old model by simulating large pressures. To study the geometrical sensitivity of the 1-day-old model, these different geometries were also investigated in terms of displacement magnitudes and spatial patterns, with the same boundary conditions and applied pressure.

Zusammenfassung

Hörschwäche ist einer der häufigsten Geburtsfehler und dessen frühzeitige Diagnose ist notwendig für eine gute Sprachentwicklung. Heutigen Testmethoden fehlt es leider an Genauigkeit und sie produzieren eine hohe Anzahl an falsch positiven Ergebnissen. Deshalb muss das Verständnis der Mittelohrmechanik bei Neugeborenen verbessert werden um Screening-Geräte und somit die Identifikation von Schallleitungshörschwäche und Zuständen wie Otitis Media (Mittelohrentzündung zu verbessern.

Ein Finite-Elemente-Modell eines 1 Tag alten Mittelohrs wurde generiert und dessen Reaktion auf einen statischen Druck von 10 Pa wurde mit der Reaktion eines bereits existierenden Modells eines 22 Tage alten Mittelohrs in Bezug auf Verdrängungsgröße und räumliches Muster verglichen. Geeignete Werte für die Materialeigenschaften wurden aus Literaturrecherchen und vorherigen Finite-Elemente Modellen entnommen. Darüber hinaus wurden unterschiedliche Geometrien des Trommelfells des 1 Tag alten Modells durch das Simulieren großer Drücke generiert. Um die geometrische Sensitivität des 1 Tag alten Modells zu untersuchen, wurden diese unterschiedlichen Geometrien ebenso in Bezug auf Verdrängungsgröße und räumliches Muster mit denselben Randbedingungen und angewandtem Druck untersucht.

Nomenclature

Symbols

A	surface area
C	damping matrix
f	force vector
K	stiffness matrix
l	length
M	mass matrix
P	sound pressure
u	nodal displacement
U	volume velocity
Z	acoustical impedance

Acronyms and Abbreviations

ABR	auditory brainstem response
AML	anterior mallear ligament
CT	computed tomography
DoF	degrees of freedom
FE	finite-element
FEM	finite-element method
Fie	fabrication d'imagerie extraordinaire

fp	footplate
MCH	Montreal Children's Hospital
OAE	otoacoustic emission
PIL	posterior incudal ligament
TM	tympanic membrane
xy-res	xy-resolution

Contents

Chapter 1

Introduction

1.1 Motivation

Hearing loss in newborns has a prevalence of around 3 in 1000 and is one of the most common congenital disorders [1]. Its early identification is crucial for further language and psychosocial development [2]. Hearing loss can be categorized into two major types: conductive hearing loss, affecting the outer and/or middle ear; and sensorineural hearing loss, affecting the inner ear (cochlea), auditory nerve (vestibulocochlear nerve) and/or the central auditory pathways in the brain [3].

Current screening tools such as auditory brainstem response (ABR) and otoacoustic emissions (OAE's), and the complementary tool tympanometry, unfortunately cannot effectively distinguish between the types of hearing loss and/or produce large numbers of false positives.

Therefore, it is important to study the newborn auditory system and of middle-ear mechanics in order to better understand the results of hearing test methods like tympanometry and common middle-ear disorders such as otitis media. However, to acquire relevant data at such an early age is difficult due to the small size of the middle ear and the major ongoing anatomical changes.

The goal of this study is to help to improve clinical tools by the use of experimental measurements encapsulated in mathematical models. The mathematical

models are based on finite-element modelling (FEM). By using FEM and assuming a relatively accurate geometry, based on X-ray computed tomography images, and relatively accurate material properties and boundary conditions, reasonably realistic simulations of newborn middle-ear mechanics can be performed.

1.2 Objectives

The first goal of this work was to generate a finite-element model of a 1-day-old middle ear and compare it to an existing model of a 22-day-old middle ear to study differences such as tympanic membrane and ossicular displacement magnitudes and spatial displacement patterns. The second goal was to characterize the sensitivity of TM behaviour to its curvature, by generating different TM shapes for the 1-day-old model and running simulations for each new shape with the same boundary conditions as in the first part of the work.

1.3 Outline of the thesis

Chapter 2 gives an introduction to the background of the investigation, including the anatomy of the auditory system and the principles of FEM. Chapter 3 presents the materials used, such as computed tomography images, and the sequence of methods used for 3-D reconstruction, mesh generation, finite-element modelling and post-processing. Chapter 4 presents the results of the 3-D reconstruction, a comparison of the models for the two different ages and the geometrical sensitivity analysis. Chapter 5 presents the discussion of the results obtained and the limitations of the study. Chapter 6 presents and overall conclusion and suggested future work.

Chapter 2

Background

2.1 Introduction

This chapter gives, first, an overview of the anatomy of the outer and middle-ear and, second, a more detailed description of the major parts within the middle ear with their roles and functions. Afterwards, the principles of finite-element modelling are briefly reviewed with emphasis on the case of middle-ear modelling.

2.2 Anatomy of the outer and middle ear

2.2.1 Overview of ear anatomy

Ear anatomy is commonly divided into three sections, the outer ear, middle ear and inner ear (figure 2.1). Generally hearing and the pathway of sound is described as follows: sound is transmitted by sound waves in the air which are captured by the pinna and forwarded through the ear canal to the tympanic membrane (TM), which is at the end of the ear canal. This leds to mechanical vibrations of the TM which are transmitted through the three connected bones (ossicular chain) to the oval window of the cochlea, which is the first structure of the inner ear. The cochlea is where the conversion of mechanical vibrations to electrical signals is actually performed by the hair cells [4]. In this manner, sound traverses air, an air-filled cavity (the middle-ear cavity) and a liquid-filled cavity (the cochlea) until the acoustical energy is converted to neural signals which are

further transported by the auditory nerves to the auditory cortex and perceived as sound.

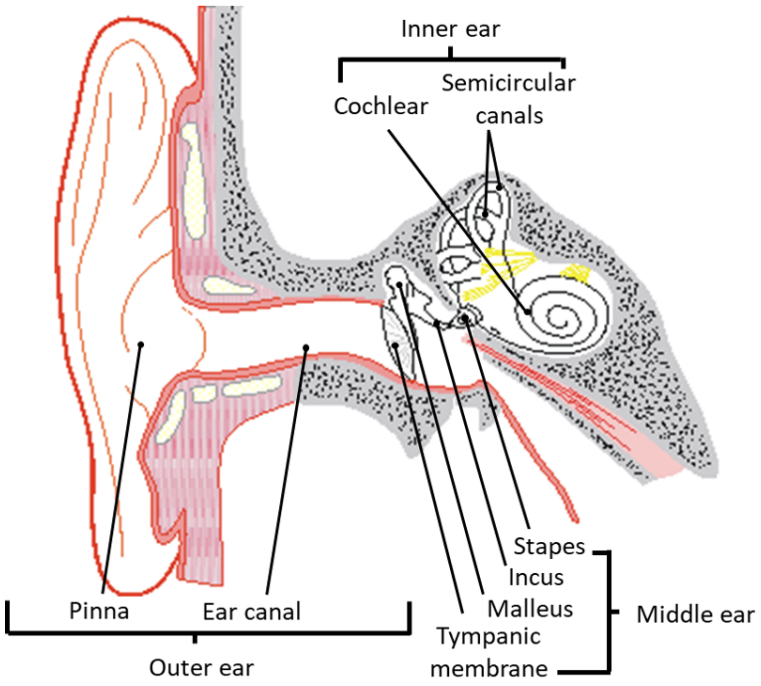

Figure 2.1: Illustration of the auditory system anatomy. After [5].

2.2.2 Pinna

The pinna, also called the auricle, was described in early studies as a funnel construction with the essential function of collecting sound and as a reflector [6]. This purpose is realized in a complex structure consisting of the helix, scapha, antihelix, concha of auricle, lobule of auricle and many other characteristics [7]. It is composed mainly of cartilage and it grows at the same rate as other components of the head and neck. At an age of approximately six to nine years the pinna has developed to its adult size [8].

2.2.3 Ear canal

The S-shaped outer ear canal in adults is approximately 3 cm long and has an average diameter of 0.6 cm. The first section of the walls are reinforced by elastic cartilage, whereas the inner section of the walls are formed by the temporal bone.

Especially the outer cartilage section contains several sebaceous and ceruminal glands which produce the cerumen (ear wax). This serves, firstly, as protection against foreign objects and, secondly, to prevent dessication of the epithelium [7]. The curvature is mainly located in the cartilage section. The ear canal is, in contrast to other parts of the middle and inner ear, not fully developed at birth and will change in the first few years. The main changes are in the shape and in temporal-bone ossification around the ear canal. At birth the ear canal is rather straight and is hardly fully ossified at all. The ear canal leads the acoustical energy to the tympanic membrane (TM) which marks the end of the ear canal and outer ear and the start of the middle ear.

2.2.4 Tympanic membrane

The tympanic membrane (TM), also called the eardrum, is a circular oval shell with an average area of 75 mm^2 [7]. It is divided into a small loose part, the pars flaccida, and a larger and stiffer part, the pars tensa (see figure 2.2). The pars tensa is funnel-shaped with the apex forming the umbo and pointing inwards to the middle-ear cavity. With a thickness of the TM pars tensa in the range of 30 to 120 μm [9, 10], one can see the shimmering stripe of the connected manubrium through the thin structure. The TM adult size is reached before birth [8]. However, the orientation of the TM plane with respect to the axis of the ear canal changes over the life span. Especially in the first three years, the angle between the canal and the TM becomes more acute. The TM pars flaccida is considered as a skin extension from the ear canal. Its thickness in adults is approximately between 30 and 230 μm [9].

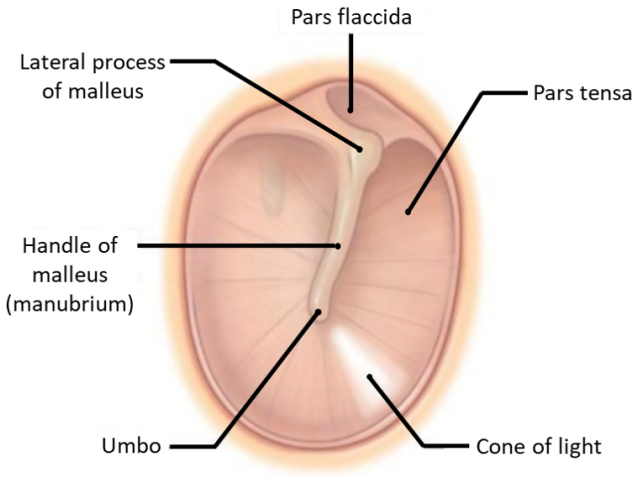

Figure 2.2: Illustration of the tympanic membrane from an external perspective. After [11].

The TM pars tensa comprises three layers: the epidermis, the lamina propria and the lamina mucosa. The outer layer, the epidermis, is similar to the epidermis of the skin in its ultrastructure. The middle layer, the lamina propria, comprises collagen fibres, which are oriented in approximately radial and circular patterns, and a loose ground matrix. The inner layer, the lamina mucosa, is thin and has a large number of columnar cells [9]. Age-related changes were reported by Ruah et al. in thickness, cellularity and vascularity. By using electron microscopy, TM structures from newborn to adult were investigated and similar age-related changes as in human skin were observed [12]. These observations are important for the material properties of the model and are further described in section 3.6.2. The mechanical properties are mainly influenced by the lamina propria, especially by its type II collagen fibre content.

The TM is fixated through the annulus fibrosus tympanicus onto the TM ring of the temporal bone. This complex connection is an extension of the connective tissue matrix of the TM [13]. Additionally, the annulus fibrosus contains smooth muscle cells which have a radial orientation [14]. This composition of tissues is

connected to the bone through a increasing thickness. Gea et al. found that this complex boundary is also deformable and cannot be simply fixed in mathematical models [15].

2.2.5 Ossicles

The ossicles, namely the malleus, incus and stapes, are the three smallest bones in the human body (figure 2.3). The most lateral bone, the malleus, is connected to the TM and comprises a head, neck, anterior and lateral process, manubrium and at the tip the umbo. As described before, the manubrium is connected to the TM along its length up to the umbo. The malleus head is connected to the incus through the incudomallear joint, the second bone in the osscicular chain. The incus is formed by a body which has a short process and a long process that leads to the lenticular process. The stapes, the third bone in the ossicular chain, is connected at its head to the lenticular process through the incudostapedial joint. From the head on, the stapes has a posterior crus and an anterior crus leading to the footplate which is in contact with the oval window of the inner ear. Noussios et al. reported in a review of literature from 50 years that measurements of the ossicular chain reveal a high variety due to differences in measurement [16]. Arensburg et al., for instance, presented a total length of 7.8±0.35, 6.4±0.24 and 3.2±0.21 mm for malleus, incus and stapes [17]. Weights and sizes of the ossicles have been reported to change with age after birth [18]. Especially the malleus and incus bone marrow is gradually replaced by bone [19].

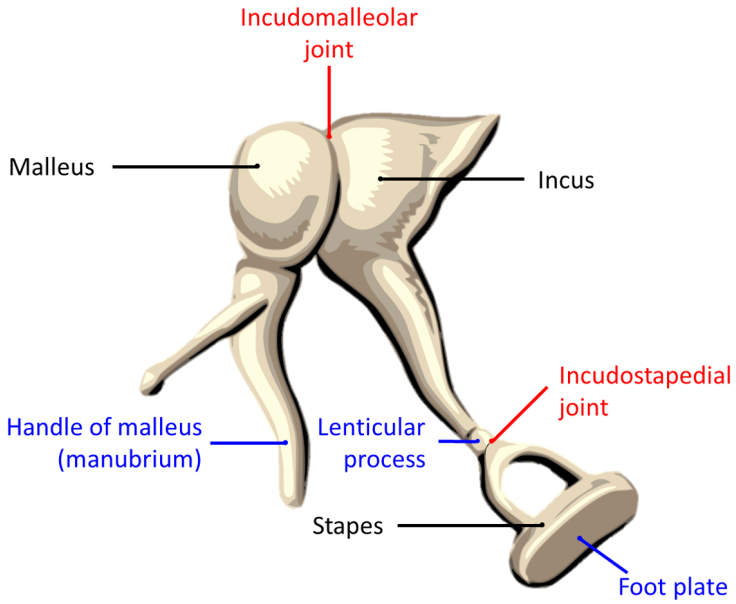

Figure 2.3: Presentation of the ossicular chain (malleus, incus and stapes). After [20]

2.2.6 Ossicular ligaments and muscles

Several ligaments suspend the ossicular chain in the middle-ear cavity. The manubrium, for instance, is connected to the TM along its length via a fibrous layer [21]. The anterior process, which is located at the malleus neck, is the point where the anterior mallear ligament (AML) is connected. Further attachment to the middle-ear cavity wall is formed by the superior mallear ligament connected to the head of the malleus. In contrast, two bundles of the posterior incudal ligament (PIL), connected to the short process, and a superior incudal ligament, connected to the incudal body, attach the incus to the cavity wall. As the last part of the ossicular chain, the footplate is connected to the oval window of the cochlea by the annular ligament. Two muscles, namely the tensor tympani and the stapedius, are also attached to the tympanic cavity wall. The tensor tympani is attached to the handle of the malleus and the stapedius muscle is attached to the stapes head. These muscles work independently and reduce the transmission of low-frequency sound like a high-pass filter [22]. They also prevent over-pressurize damage of the inner ear by stiffening the ossicular chain.

2.2.7 Middle-ear mechanics

As described before, the middle-ear transmits sound vibrations in the air through the TM and ossicles to the cochlea. Middle-ear function can also be described as a transforming function in which it matches the low acoustical impedance in air to the high acoustical impedance in the liquid of the cochlea. Acoustical impedance is a measure to describe how much resistance a sound wave encounters when passing through a medium such as air, liquid or tissue. This is defined as

$$Z = \frac{P}{U} \tag{2.1}$$

where Z is acoustical impedance, P is sound pressure and U is volume velocity. This equation can be used to calculate how well an acoustical wave is transmitted or reflected at borders of media with different acoustical impedances. This impedance is bigger in a liquid than in air. This means that a large amount of sound energy that is transmitted through the middle ear (air pathway) to the cochlea (liquid pathway) will be reflected. For this reason, the middle ear has, in addition to a transmission function, a matching mechanism which is often described as working based on three principles: a surface area ratio, a lever-arm ratio and a TM curvature (figure 2.4).

This matching mechanism is mainly based on the surface ratio formed by the TM surface area and the stapes foot plate surface area. Since the force applied on the TM is almost the same as that transmitted to the footplate, the pressure that is applied on the TM surface is through this principle not only transmitted to the footplate, but increased by a factor approximately equal to the ratio of the two areas (A_{fp}/A_{TM}). The effective surface area of the TM is considered to be around two thirds of the whole surface, approximately 55 mm^2, whereas the footplate effective surface is considered to be around 3.2 mm^2, when moving in a piston-like fashion (as cited by [23]). In this manner, the pressure on the stapes footplate is around 17 times as hight as the pressure applied on the TM.

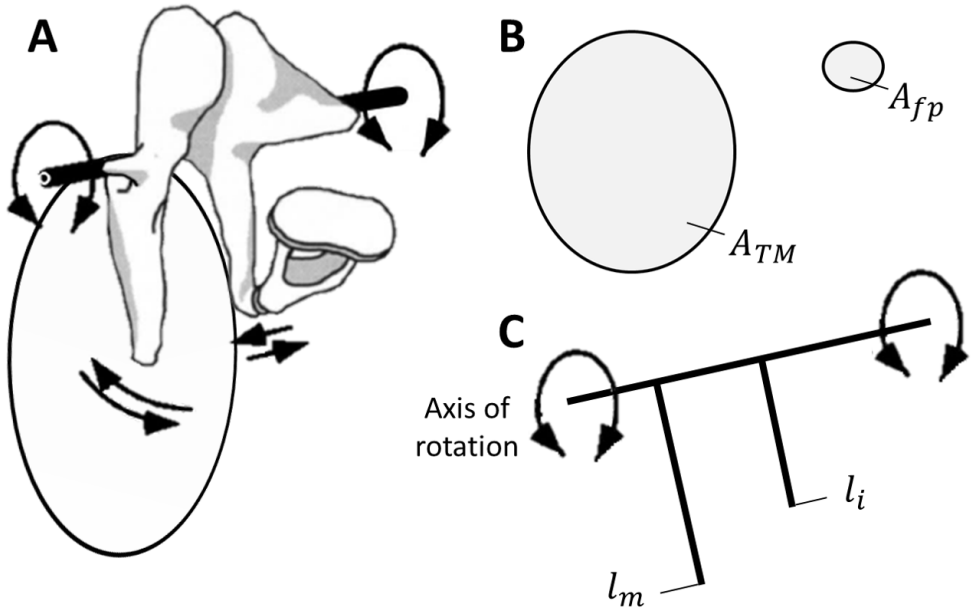

Figure 2.4: (A) Illustration of the middle ear highlighting the movements by arrows and around the rotational axis formed by the anterior mallear ligament and the two bundles of the posterior incudal ligament. (B) Presents an approximation of the surface-area ratio with A_{TM}=surface area of TM and A_{fp}=surface area of foot-plate. (C) Depcition of the lever-arm action of the middle ear with the ratio of l_m=lever length malleus and l_i=lever length incus. Panel A after [24]

The second principle is enabled by the different lever-arm lengths of the manubrium and the incus. By the applied force on the umbo with a lever (manubrium), the mechanism works like a mechanical lever action around the fulcrum (rotational axis) formed by the AML and the PIL. Since the incus is connected to the same fulcrum with a smaller perpendicular lever length (long process of incus), the force is increased and transmitted to the stapes. Plausible ratio values (l_i/l_m) from 0.5 to 0.77 have been reported [25, 26].

The last transformer principle is known as the curved-membrane effect and was hypothesized by Helmholtz (1868) and further mentioned later by Tonndorf and Khanna [27, 28]. Helmholtz stated that the amplification was caused by the TM fibre arrangement and curvature and proposed the requirement of TM tension and anisotropy. In contrast to Helmholtz, Funnell reported a more effective manubrium movement due to forces at certain areas of the TM based on the curvature dependency of TM, but without a need for TM tension and anisotropy [29].

It is difficult to specify the exact contribution of each principle separately due to the linkage and dependency of all principles to the TM material properties and geometry [29]. Therefore, it is even more important to develop an understanding of the TM curvature effects. Furthermore, the mechanical behaviour is defined also by the rotational axis formed by the AML and PIL. This axis depends on the frequency and intensity of the incoming sound wave and changes as those factors change. On the whole, all of them play an important role and are involved in the impedance-matching mechanism of the middle ear.

2.3 Finite-element method

2.3.1 Principles

The finite-element method (FEM), a type of distributed-parameter modelling, is based on breaking down a complex structure, which is mathematically difficult to solve, into a large number of finite and simple elements which are readily solved. In this manner, the behaviour of complex systems with irregular geometries and boundary conditions can be described by solving each finite element individually and assembling them back together to represent the whole system. The finite-element method can be broken down to three principle steps:

- **Pre-processing**
  Discretizing into finite elements by generating a geometry and a mesh. Allocation of material properties, boundary conditions and loads to each element resulting in mathematical formulations.
- **Processing**
  Solving the mathematical formulations.
- **Post-processing**
  Evaluating and validating the results.

These elements can be multidimensional, have different types of topology and be linear or higher-order. For reasons such as adaptability to specify any geometry and computational simplicity, triangular (2-D) and tetrahedral (3-D) elements

are often used. Each element is described by a force-displacement relationship which is analysed by the responses at the discrete nodes. For static problems this force-displacement relationship is formulated as

$$Ku = f \tag{2.2}$$

where K is the known stiffness matrix of the element, u is the nodal displacement vector and f is the vector of applied nodal forces. This is rearranged to get the unknown displacement. In the case of a dynamic problem in a FEM system the equation is

$$M\ddot{u} + C\dot{u} + Ku = f(t) \tag{2.3}$$

where M and C are the the mass and damping matrices.

Nodes and elements

Nodes in FE models are locations in space with specific coordinates. They have defined degrees of freedom (DoF) which can be translational or rotational.
The order of elements describes the interpolation function, for instance, along the edge of elements. First-order elements (linear) have no nodes within the edges, whereas second-order elements (quadratic) have an additional node in the middle of the edge. By the use of higher-order elements, such as quadratic, not only the number of required elements but also the approximation error can be reduced [30].
Another important factor is the element aspect ratio that can lead to numerical problems when too high and not considered. This is the measure of how equal the lengths of the edges are. Elongated thin and long elements have high aspect ratios.

2.3.2 Finite-element modelling of the ear

The use of FEM to analyse the eardrum function and structure was first performed by Funnell (1975) and subsequently improved in 1978 by modelling the

cat eardrum (Funnell and Laszlo) [31, 32]. They modelled the cat TM as a thin shell and analysed its static response. The extension of this model with investigations on the response of higher frequencies without damping were presented by Funnell in 1983 and including damping effects by Funnell et al. in 1987 [33, 34]. From there on, many studies were conducted to investigate human and animal middle-ear mechanics in the linear and non-linear regimes by the use of FEM. It was reported already in early studies that the most influential factors in the middle-ear model are the TM curvature and its anisotropic material properties [29, 32]. How sensitive the model is to its geometry and which curvatures drive the ossicles more or less, is not often well investigated. In a recent study, De Greef et al. presented FE modelling of three different geometries with the same simulating parameters and found that it can lead to significantly different responses [35].

Qi et al. reported the first newborn ear-canal finite-element model focusing on soft-tissue deformation in response to high pressures [36]. In 2008 they presented investigations on the newborn middle-ear in the non-linear regime with its response to high pressures [37]. Based on these models, with new material properties from experimental data and with a revised and more accurate TM thickness, Motallebzadeh presented a more recent finite-element model of the newborn middle ear [38, 39].

2.3.3 Low-frequency simulation

In a low-frequency simulation it is assumed that the input frequency of the sound pressure waves are low enough to neglect damping and inertial effects. This simplification allows us to obtain results by using static inputs without all the transient behaviour of dynamic simulations. Therefore, a static pressure is used in this study without consideration of damping and inertial effects, which are frequency dependent. This refers to the force-displacement relationship as formulated in equation 2.2.

Chapter 3

Materials and Methods

3.1 Introduction

This chapter will describe the data sources that were used, the methods by which the 3-D model was developed, which material properties and boundary conditions were used, and finally how the finite-element modelling and sensitivity analysis were performed.

3.2 CT scans

The 3-D reconstructions of the newborn middle ears were based on X-ray computed tomography (CT) scans obtained from the Montreal Children's Hospital (MCH). CT scans are not lightly made for newborns due to radiation exposure. These CT scans were made for the two babies at the ages of one day and 22 days, respectively, due to indications of hearing loss or malformations of the ear and insufficient data from other tests (table 3.1). CT scans can provide a detailed image of the inside of the body, especially of bony structures. The scans were performed along the patient in the transverse plane, producing a cross-sectional view (Figure 3.1). The image series were obtained from a LightSpeed 16 CT scanner model from GE Healthcare (General Electric Company, USA) and were provided in 'JPG' format. With a focus on the mastoid, around 40 to 60 image slices of the inner, middle and outer ear were imaged per patient. Each image slice has a pixel size of 0.1875×0.1875 mm. The slice thickness was 0.625 mm

and the slice spacing was 0.5 mm. A helical scan mode with an exposure time of 1260 ms was used. An example CT slice of the 1-day-old infant focusing on the left ear is depicted in figure 3.1A. Figure 3.1B illustrates the procedure and the spatial orientation of the CT slices in a schematic. For the 1-day-old the left ear and for the 22-day-old the right ear was found clinically to be normal in terms of anatomy and hearing, and those are the ears modelled here.

Table 3.1: Patient specifications.

Information	**Patient A**	**Patient B**
Sex	Male	Male
Age	1 day	22 days
Number of images	41	57
Year of imaging	2004	2005
Additional patient history	Right ear malformation	Absent left ear canal
Patient position	Head First-Supine	Head First-Supine
Ear modelled	Left	Right

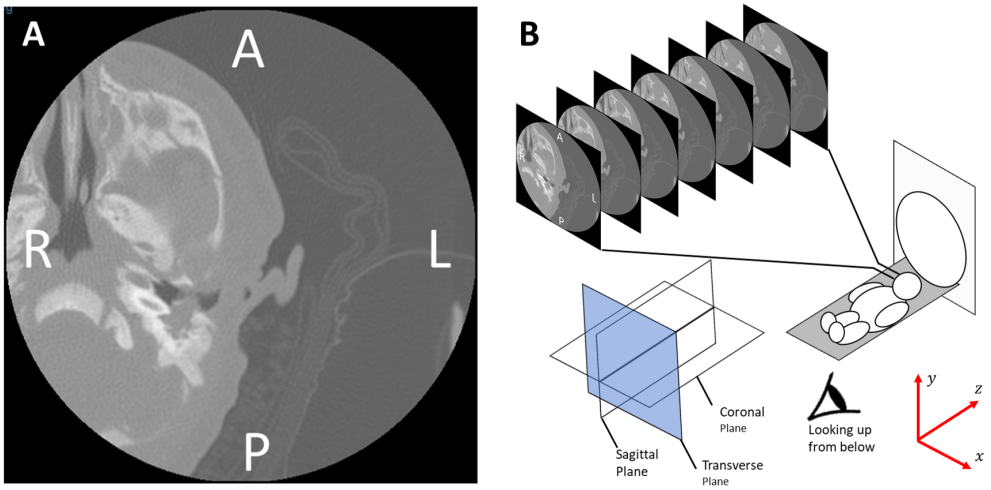

Figure 3.1: (A) CT scan image of the left ear of the 1-day-old infant. A=anterior, P=posterior, R=right and L=left. (B) A series of CT scan images of the 1-day-old infant in the direction of imaging. The images were made in the transverse plane looking up from below (transverse plane looking from feet to head).

3.3 State of models and CT scans

Previous students worked on both models with different goals and different finite-element solvers.

3.3.1 22-day-old model

Previous studies of this model were published by Qi et al. and Motallebzadeh et al. [40, 41]. Therefore, most of the parts which were needed for this study were already segmented but for different purposes, like ear-canal and middle-ear cavity investigations. More specifically, TM and ear-canal volume displacements were examined. To provide the same conditions in terms of model parts, mesh resolution and material properties, several parts were revised, optimized and updated. Furthermore, the model was run by Qi et al. and Motallebzadeh et al. using COMSOL^{TM} (http://www.comsol.com) and Code_Aster (http://www.code-aster.org/), respectively.

3.3.2 1-day-old model

Many elements in the 1-day-model were already segmented, but without clear structure and consistency, which caused many errors. Therefore, the whole model was cleaned or refined and most of the important parts were segmented again.

3.3.3 CT scan comparison

The CT scan quality and ease of segmentation for the two models were compared. The following image series (figures 3.2 and 3.3) show the CT scans for both ages at comparable depths. The image series A presents the 1-day-old and series B presents the 22-day-old infant. To highlight the differences, an additional image of the middle-ear cavity is magnified for both ages with the same scale and size.

Comparison figure 3.2 panels A1 and B1 show the location of the middle-ear cavity at a depth where the malleus and the incus start when going from top to bottom in a transverse plane. The scale and size of the magnified image with the red frame is the same for both ages. The middle-ear cavity differs in size but

also in contrast. The 1-day-old ear seems to have fluid or mesenchyme (tissue) around the ossicles. This can also be observed in the second pair of CT scans (figure 3.2 A2 and B2) at the depth of the posterior incudal ligament. Again the cavity size of the 22-day-old model is bigger and the higher contrast allows a better identification of the anatomical structures. The third pair of CT scans (figure 3.2 A3 and B3) depicts the transition between pars flaccida and pars tensa and the start of the manubrium. This pair shows the same differences as the first two pairs.

Figure 3.3 shows three more CT scan pairs focusing on the TM at different depths. The first pair (A1 and B2) depicts the manubrium and the TM at both ages. Unlike the 22-day-old, the 1-day-old middle-ear cavity is predominantly filled with fluid or tissue. The TM is not clearly visible but a separation between middle-ear cavity and ear canal is possibly indicated by the boundary of the fluid or mesenchyme. The manubrium is hardly visible. In contrast, the 22-day-old shows a clear manubrium. Although the TM is a non-bony and thin structure, the scan of the 22-day-old indicates its location in the first pair and shows landmarks (L in the figure) in the second pair of CT scans. Even the third CT scan (B3) shows connections to the temporal bone and a curvature in the centre of the magnified image. On the contrary, the 1-day-old second image (A2) shows the middle-ear cavity with blurred contours which might show part of the TM. In addition, images A3 and B3 depict the middle-ear cavity coming to an end with possible indications and landmarks of the TM for both ears.

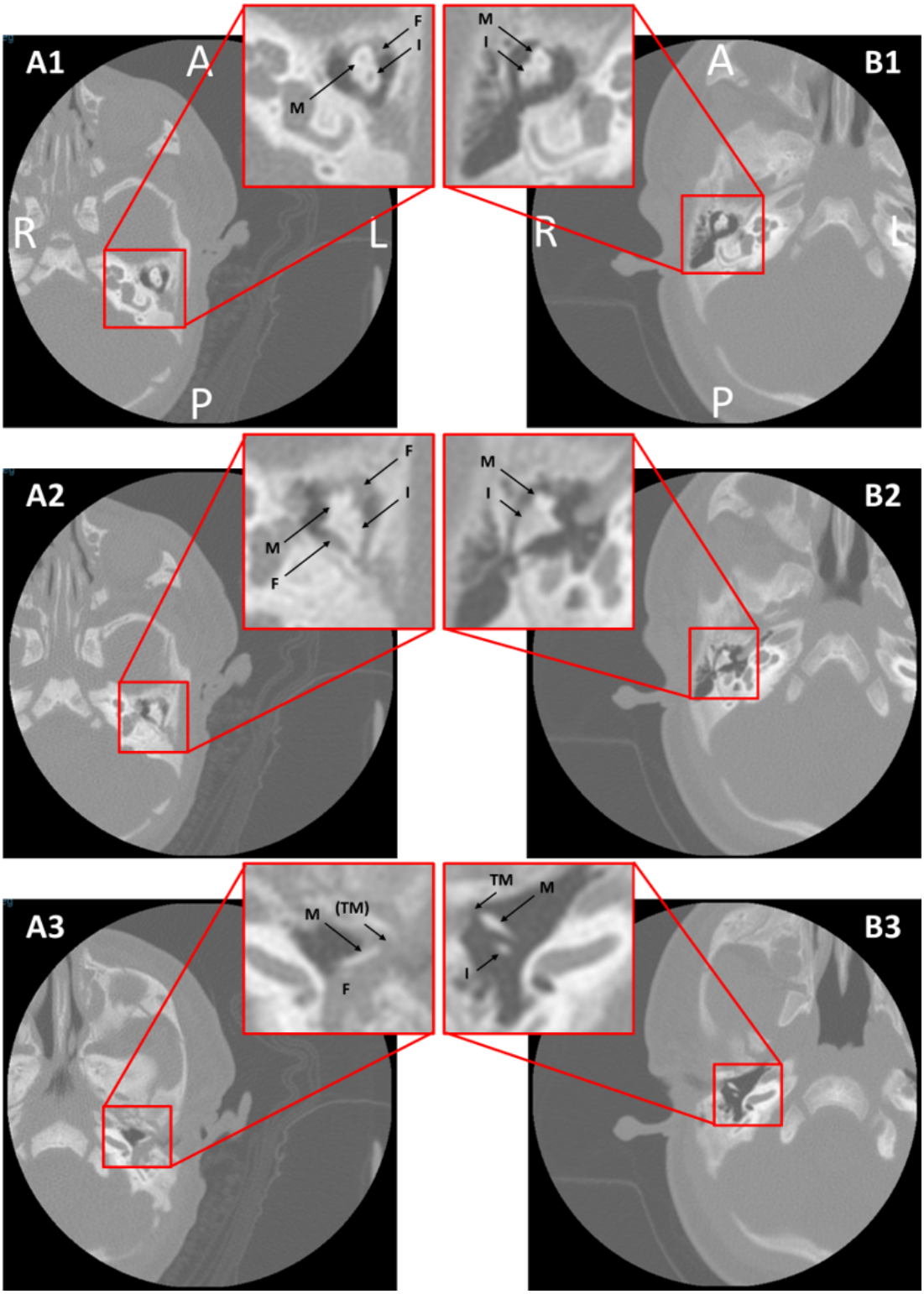

Figure 3.2: Image pairs illustrating CT scans of the 1-day-old (A) and the 22-day-old (B) infants at comparable depths. The first CT scan pair shows the orientation with A=anterior, P=posterior, R=right and L=left. In addition, an image focusing on the middle-ear cavity is magnified with the same scale and size for both ages. Anatomical structures and attributes are indicated in the magnified images with M=malleus/manubrium, I=incus, TM=tympanic membrane and F=fluid.

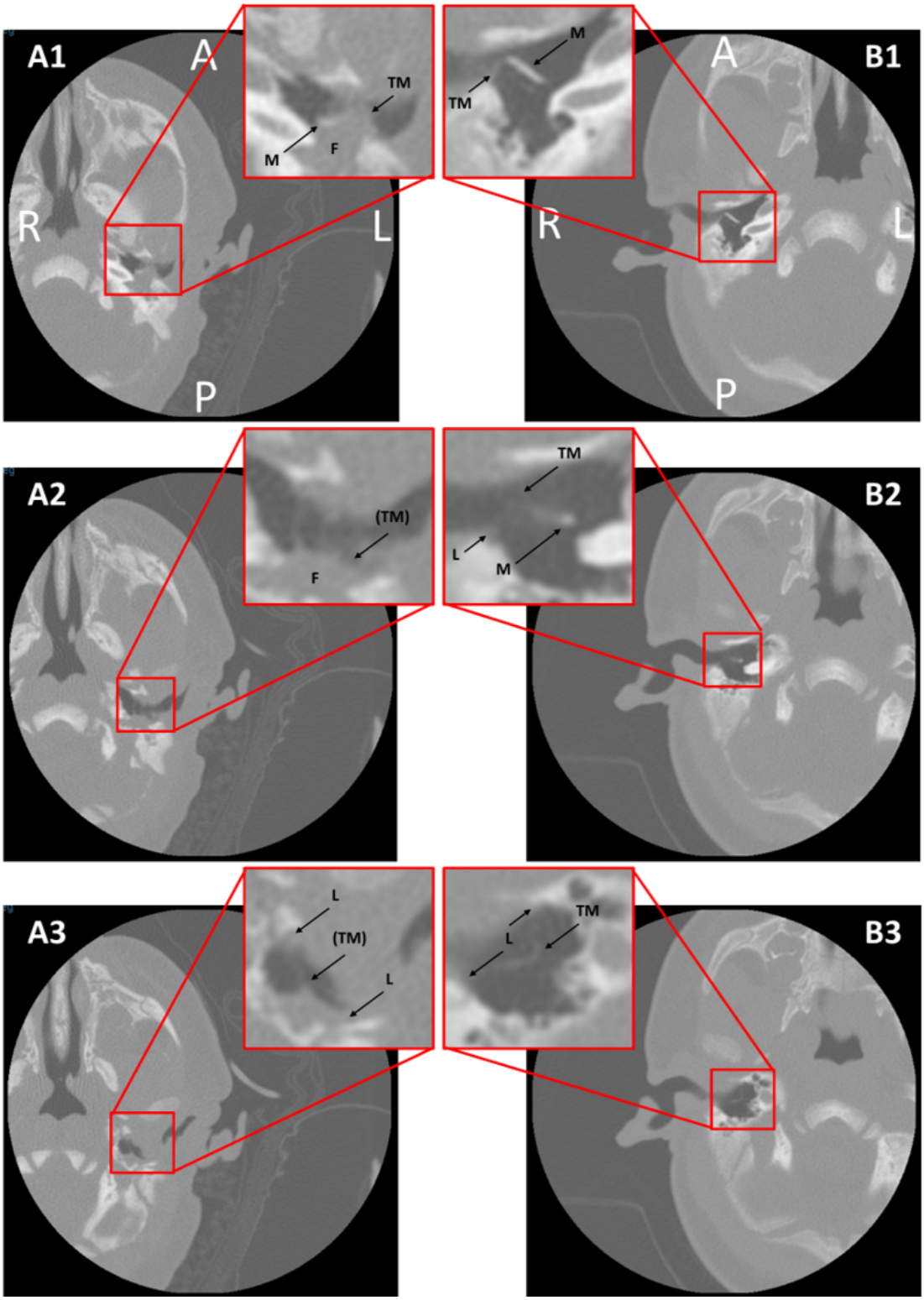

Figure 3.3: Second series of image pairs illustrating further CT scans of the 1-day-old (A) and the 22-day-old (B) infants at comparable depths. The first CT scan pair shows the orientation with A=anterior, P=posterior, R=right and L=left. In addition, an image focusing on the middle-ear cavity is magnified with the same scale and size for both ages. Anatomical structures and attributes are indicated in the magnified images with M=malleus/manubrium, I=incus, TM=tympanic membrane, L=landmarks (see text) and F=fluid.

3.4 3D reconstruction and model components

For the 3D reconstruction of the middle ear, four locally developed computer programmes were used. Fabrication d'imagerie extraordinaire (Fie), Tr3, Thrup'ny and Fad (McGill University Department of BioMedical Engineering, Auditory Mechanics Laboratory, http://audilab.bme.mcgill.ca/sw/). The sequence of the procedure is presented in figure 3.4.

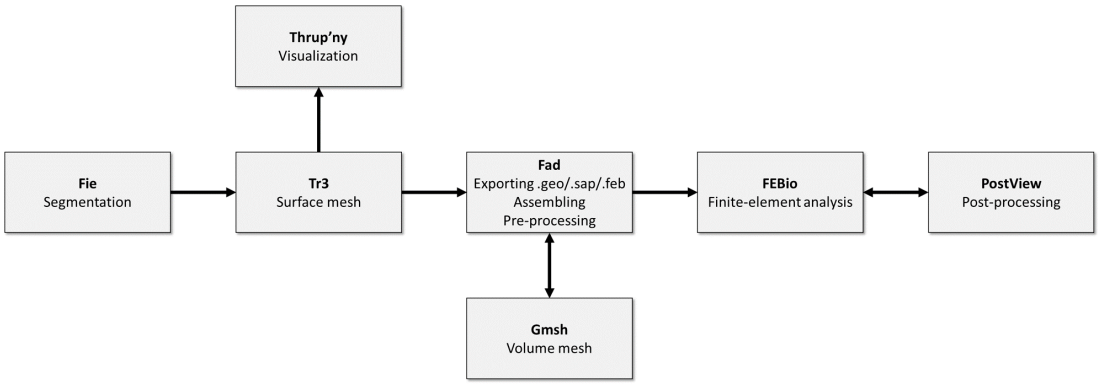

Figure 3.4: Schematic of the sequence of model creation and simulation.

The CT images were imported into Fie. Each CT image was viewed separately for desired anatomical structures like TM, malleus, incus or stapes. The contours of these regions of interest were then traced by connected nodes. Figure 3.5A shows an example where the ear canal is traced in brown, connected to the TM in green sharing the surface with the manubrium of the malleus (beige) next to the incus tip (green). The graphical user interface of Fie is shown in panel B with another CT image in the main window (x-y image), the side views in two windows below (x-z image on the left and z-y image on the right). The main functionalities are arranged in the menu on the left.

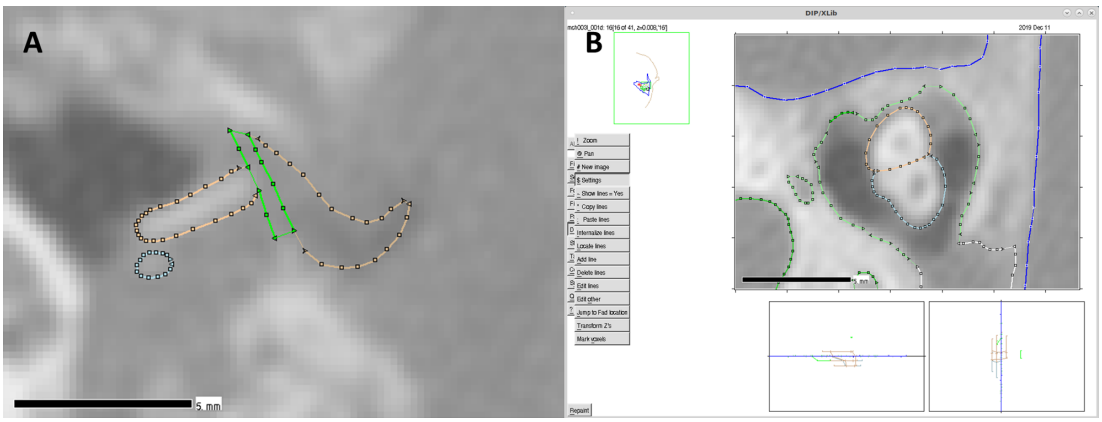

Figure 3.5: Segmentation of CT images using the Fabrication d'imagerie extraordinaire (Fie) software (http://audilab.bme.mcgill.ca/sw/fie.html). (A) A CT image of the 1-day-old infant with segmented ear canal (brown), tympanic membrane (green), malleus (beige) and incus (blue). (B) The graphical user interface of Fie during segmentation of anatomical structures of a CT scan from the 1-day-old infant. This CT image includes the malleus head (beige), incus head (light blue), temporal bone (blue) and middle-ear cavity partially in green and white. The scale bar in both images shows a distance of 5 mm.

Several rules, such as tracing direction, tracing start and finish points, joins and caps were considered for the segmentation to get a smooth model without triangulation and mesh errors. Segmentations are performed either (1) manually, or (2) automatically by setting the start point along a boundary or by defining a range of pixel intensities of a closed region. Regardless of which method was used, the segmentation line can be adjusted afterwards manually or by smoothing functions. Mostly manual segmentation was used and was necessary due to low-contrast structures and poor image resolution. Depending on whether it is a solid structure or a cavity, the segmentation is performed counter-clockwise or clockwise. Furthermore, each segmentation line has many attributes including line colour, mesh resolution and simulation-related attributes like material type, boundary condition and thickness. Structures which appear in some slices as single and closed may appear in other slices as divided or may share a surface with another structure. In this case the line name was changed with the change in the nature of the structure, with the corresponding slice number included in the line name. Several segmentation lines that describe the same structure, such

as the malleus, can be combines in one subset. In addition to the CT scans, published literature and histology slices of a 1-day-old were used for the difficult structures which were not well imaged. These gave, for instance, supplementary insights about the orientation and thickness of the TM as seen in figure 3.6. The malleus was identified well in nine slices and with difficulty in 2 additional slices, and the incus in eight slices. Often the accumulation of amniotic fluid or mesenchyme at the boarder of the middle-ear cavity and the ear canal indicated the location of the TM. In contrast to the AML, the PIL was sufficiently visible in two slices. The AML was segmented based on landmarks from histological images. Figure 3.6 illustrates histological sections which were used with the CT scans for the TM segmentation. They indicated possible landmark positions and TM thickness. Finally, the 3-D reconstruction comprised the TM, malleus, incus and the ligaments (AML and PIL).

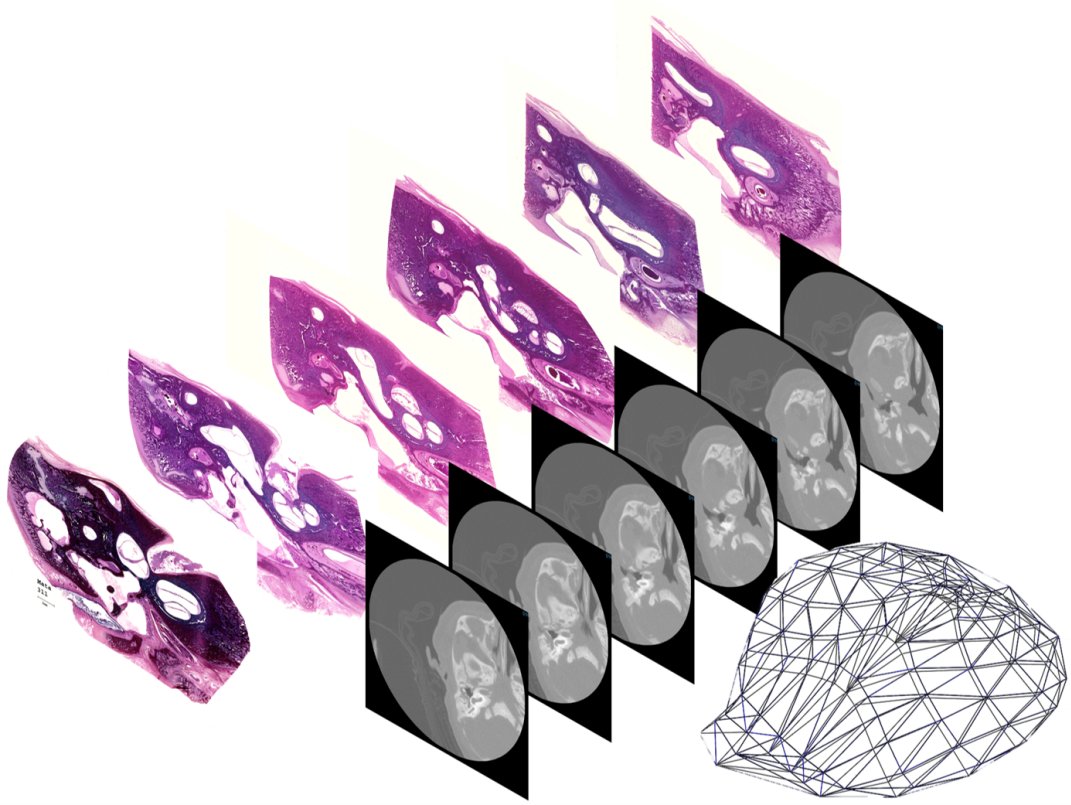

Figure 3.6: Illustration of histological images and CT scans (mirrored) from two different 1-day-old infants and the segmented 3-D model of the tympanic membrane in wire-frame style. Histological sections were used as supplements to the CT scans to obtain information about landmarks, TM thickness and ligament location.

The segmentation in Fie resulted in a single '.tr3' file for all parts of the middle ear, which was then imported to Tr3. This software was used to develop a surface mesh out of the 2-D segmented images by connecting the contour lines of different slices with triangles (figure 3.7). The triangulation of each segmented line pair, join and cap could be accepted or modified using the Tr3 verification option.

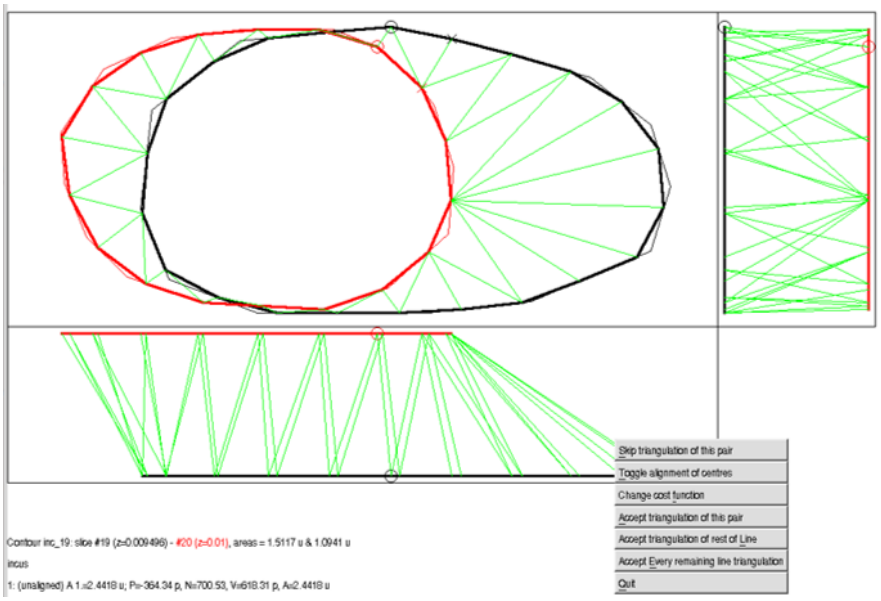

Figure 3.7: Triangulation between lines traced from the segmented CT images by using Tr3 (http://audilab.bme.mcgill.ca/sw/tr3.html). The software connects the segmented lines from the different slices with a triangle mesh to build a 3D model. In this case, the triangulation of two malleus lines (black line in slice 19 and red line in slice 20) is illustrated in three orthogonal planes. The verification option (grey tab) allows modification or acceptance of line pairs.

The resulting 3-D model was exported as a 'VRML' file for visualization with Thrup'ny and as a '.sap' file for further processing with Fad. By constantly checking the 3-D model in Thrup'ny and adjusting the segmentation in Fie, the best possible geometry was developed in an iterative process. Figure 3.8 shows the visualization of the malleus subset in Thrup'ny in the default style in panel A and in the wire-frame style in panel B.

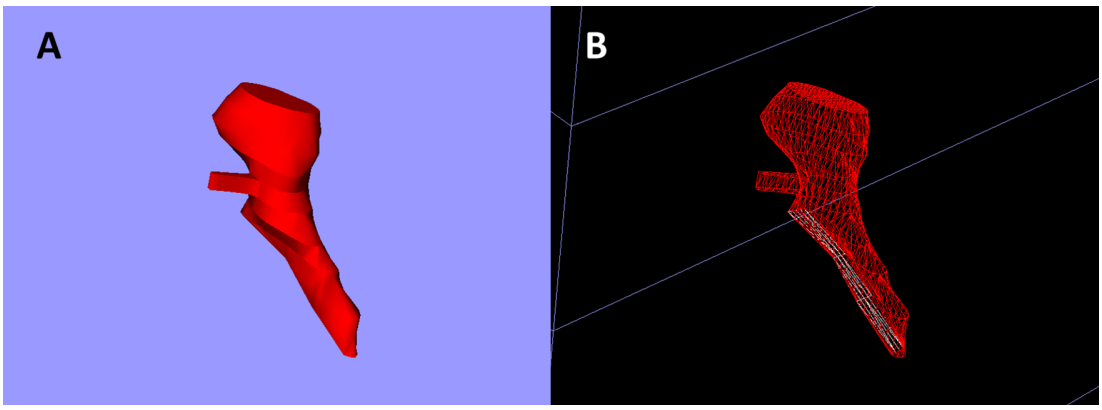

Figure 3.8: Visualization of the 1-day-old infant malleus 3D model examined by Thrup'ny (3D viewer software, http://audilab.bme.mcgill.ca/sw/ thrupny.html). (A) The default 3D model view of the malleus, (B) The wire-frame style highlighting the triangulated mesh structure of the malleus.

Fad is also used in between the different applications to export the data in the right format, and more importantly it is used to detect high aspect ratios within the model. High aspect ratios occur when the the elements are elongated, long and thin. They can cause numerical problems and thus need to be corrected in Fie when identified.

The 3-D reconstruction of the middle-ear comprises the TM (consisting of pars flaccida and pars tensa), malleus, incus, AML and two bundles of PIL. It was assumed that the incudomallear joint is fused so there is no motion between these ossicles. This simplification was used in previous investigations for the 22-day-old model [40]. Furthermore, Dirckx and Decraemer reported in an experimental study that the stapes had only a small influence on the TM deformation, which is why it was not included in previous investigations in the 22-day-old model [42]. Additionally, the CT resolution made the segmentation of the stapes difficult, which is why it was not included in this investigation either.

3.5 Mesh generation and convergence

Mesh quality is crucial for finite-element modelling and affects the solution accuracy. The coarser the mesh the less computation time is required, but for a less accurate solution. Conversely, the finer the mesh the greater the computational

time is and the more accurate is the solution.

The resolution in the *xy* plane as *ires_xy* and the resolution in the *z* direction as *ires_z* were setting attributes which were defined for each line in Fie. The *ires_xy* parameter is measured in elements per diameter, while the z-resolution is measured in slices. The *ires_xy* value was used to change the xy-resolution of the mesh in order to investigate mesh resolution effects on the simulation results. By defining *ires_xy* equal to 20, for example, the triangle elements will be scaled to fit approximately into 1/20 of the overall segmented diameter. This works by redividing the segmentation lines so that the desired triangle size is achieved. In Fie, the mesh resolution parameter *ires_xy* is by default set to 0, which means that Tr3 uses all the nodes which were segmented without redivision. Since the *ires_xy* parameter defines the xy-resolution of the mesh, the expression "xy-resolution" (xy-res) is used instead in the following. In contrast, the number of slices is limited and is provided by the CT. Therefore it is not possible to increase it, but by setting the parameter *ires_z* of a segmented line to 2 would result in taking only every second slice into account.

A convergence study was performed to find a mesh resolution with a good trade-off between the most accurate solution and the least computational expense. The focus of this study was the TM (pars flaccida and pars tensa) mesh. Therefore, a range of xy-resolution values was used to identify the optimal resolution based on the resulting total displacement values for the TM. The increased mesh resolution should achieve an asymptotic increase in displacement accuracy but also result in an increased computational expense. Therefore, a TM model with the initial state (i.e., xy-resolution=0 and thus only the segmented nodes) was generated and compared with additional TM models with increased xy-resolution.

To generate a tetrahedral volume mesh from the triangulated surface mesh, Gmsh (http://www.geuz.org/gmsh/) was used separately for each individual model of the middle ear. According to the mesh resolution of the surface, the resulting volume mesh is either fine or coarse. As seen in figure 3.9, the malleus surface mesh is transformed to a solid model with a tetrahedral mesh inside the malleus.

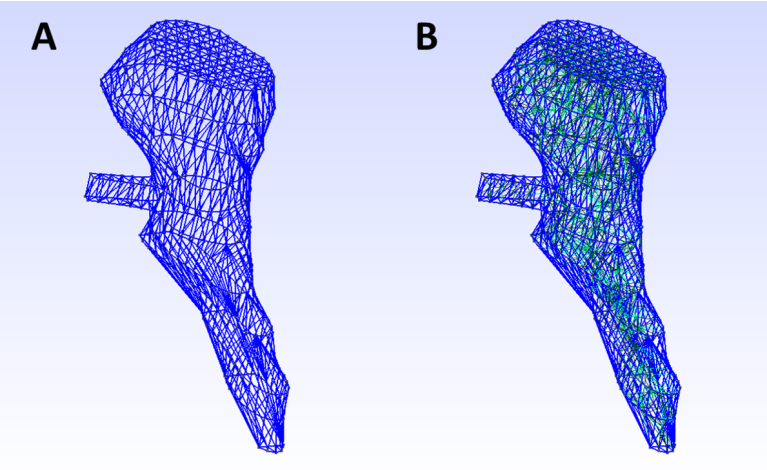

Figure 3.9: Illustration of the malleus in wire-frame 3D visualization with volume mesh generator Gmsh (http://www.geuz.org/gmsh/). (A) The triangulated surface mesh, and (B) the generated tetrahedral volume mesh.

After the volume mesh generation for each part of the model, Fad was used to assemble the individual tetrahedral models together one by one. During this procedure Fad identified interface nodes and combined them. The maximal allowable distance was set and afterwards the user confirmed that the actual maximal distance was zero (see figure 3.10). After each part had been joined to one complete model, the orientation was changed in Fad to make the results reproducible and comparable. More specifically, the TM was aligned parallel to the xy plane for both models. In this manner, the main TM displacement was in the z direction.

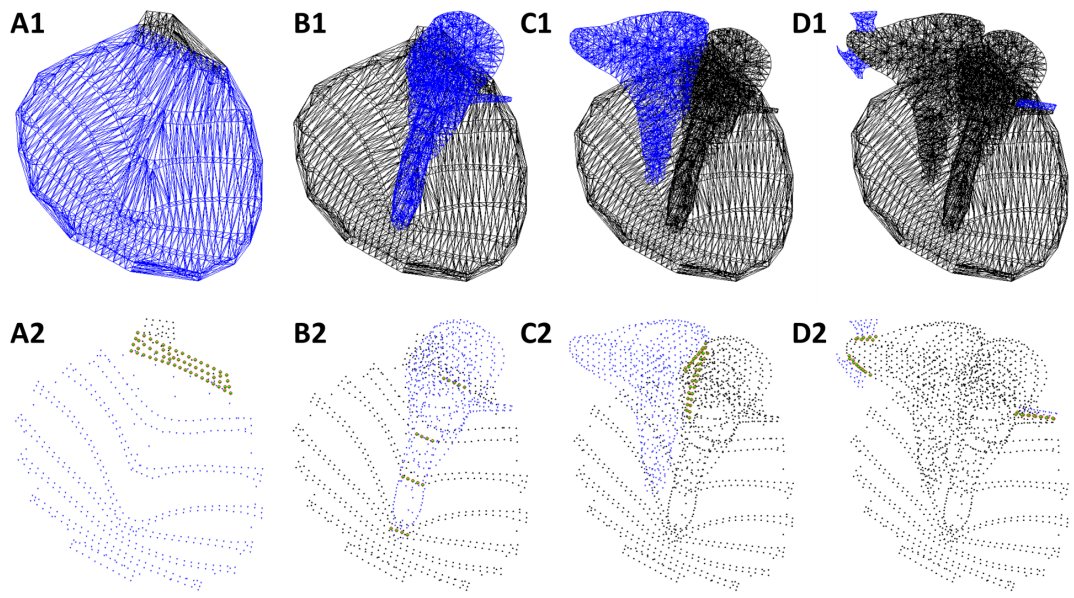

Figure 3.10: Visualization of the model assembly with the join command of Fad (http://audilab.bme.mcgill.ca/sw/fad.html). After the volume mesh was generated for each part, they were joined together one at a time. The blue part is the newly joined part which is the pars tensa in (A), the malleus in (B), the incus in (C) and the ligaments in (D). (1) depicts the wire-frame view and (2) the nodal view with all identified interface nodes in green and red.

In the convergence study, only the TM pars flaccida and pars tensa were joined together. In this manner, the finite-element analysis was performed only on these two parts, with the same material types and boundary conditions but with different mesh resolutions in order to examine only the influence of mesh resolution.

3.6 Material properties

Middle-ear material properties have been investigated for a long time. However, definitive values are hard to determine. Reported values show wide variations due to challenges related to material property measurements of biological tissue. Controllable experimental variables like tissue state, temperature, time to death or tissue excision, experimental method used and whether in vivo or ex vivo make it difficult to compare the results [43]. For instance, the TM, with its extreme thinness and its complex fibre organization is difficult to measure.

Material properties of newborn tissues are even more difficult to obtain. When choosing material properties it is important to know whether the system is in the linear or non-linear range. Since the simulations here are performed with a constant load of 10 Pa (113.9 dB SPL), there will be no large deformations that will push the system into the non-linear range. Furthermore, in this work only a static input pressure will be used, and thus time-dependent effects such as inertia and damping can be neglected. Appropriate values were taken from literature reviews and previous finite-element models .

3.6.1 Poisson ratio and mass

The Poisson ratio describes the compressibility of a material and usually ranges from zero (such as for cork) to 0.5 (for an incompressible material). As in many previous studies [24, 44, 45] a Poisson ratio of 0.3 was taken for the ossicles. Since soft tissues are nearly incompressible, a higher value close to 0.5, specifically 0.485 [36, 41, 46], was chosen for the ligaments and the TM.
Motallebzadeh et al. [41] reported a density (mass per unit volume) of 1200 kg/m^3 for tissues and a density of 2000 kg/m^3 for the ossicles, which were also used for this project.

3.6.2 Young's modulus

Tympanic membrane

Ruah et al. [12] found, after investigations of the newborn and adult TM with light and electron microscopy, that with age the TM gets less cellular and vascular. Furthermore, they reported that with age the TM has more collagen fibres and elastin. These changes in structure and properties were described in further studies as including changes of water content and changes of density and orientation of the collagen fibres [47, 48]. Based on these reports, values half the size of those for adults were taken. Specifically, stiffnesses of 10 MPa and 2 MPa were taken for the pars tensa and pars flaccida, respectively, similar to the values used by Motallebzadeh et al. [41].

Ossicles

Olszewski et al. showed that the ossicles continue to develop after birth, with changes in mass and size [18]. The bone marrow in the malleus and incus changes gradually to bone [19]. Therefore, a smaller stiffness than that in adults has to be considered. Soons et al. measured an average stiffness of 16±3 GPa for the malleus and incus of a rabbit [49]. In another study, De Greef et al. used a Young's modulus of 14.1 GPa [35]. Considering these observations and values mentioned in the literature, a Young's modulus of 13 GPa was chosen for the ossicles in this study.

Ligaments

In previous studies, a wide range of values from 0.65 to 21 MPa were used for the ligament stiffness in adult models [24, 50]. For this study, the same value as in Motallebzadeh's report, namely 8 MPa, was chosen for the ligaments [41].

Table 3.2: Material properties.

	Young's modulus (MPa)	Poisson ratio	Density (kg/m3)
Pars flaccida	2	0.485	1300
Pars tensa	10	0.485	1300
Ossicles	13000	0.3	2000
Ligaments	8	0.485	1300

3.7 Boundary conditions and load

Boundary conditions and pressure loads are specified for each line in Fie and then ultimately are applied by Tr3 to specific nodes in the finite-element models. In the case of attributes which are valid for all segmentation lines of one individual model, they can also be defined in the subsets. Pressure and whether nodes are clamped or free were defined.

The TM border ring that is connected to the bone is clamped at all nodes. Furthermore, for the ossicular rotational axis, the ends of the AML and the two bundles of the PIL were fixed as well. All other parts of the model are free to move. The sound pressure of 10 Pa was applied on the lateral side of the TM pars flaccida and pars tensa. Since the pressure is considered to be static, there are no damping or inertia effects. This simplification is adequate for frequencies up to a few hundred Hz.

3.8 Finite-element method

FEBio version 2.9 (https://febio.org/), open-source software for biomechanical finite-element analysis, was used as the finite-element solver. At first the simulations were done with one layer of linear elements for the TM. Since a quantitative simulation needs at least three to five layers of linear elements to give adequate accuracy, the mesh was later converted by Fad to a more accurate element type, namely quadratic elements.

For the 1-day-old model, 1037 nodes were used with the linear elements before converting to quadratic. After conversion, the model had 6217 nodes. The 22-day-old model had 805 nodes with linear elements and 4793 nodes after conversion to quadratic elements.

Loads of 1 to 1000 Pa were used to identify at which point the model reached a non-linear regime. Further simulations were run with 10 Pa which is in the linear range.

After solving the finite-element model, the post-processor PostView (https://febio.org/postview/) was used to look at the displacements and deformations of the models. Additionally, the displacement at specific nodes were observed with the post processor.

3.9 Geometry development and sensitivity analysis

In order to study the sensitivity of the model to its geometry, and specifically the effects of the curvature of the TM, the segmented model was taken as a baseline and the TM shape was changed by using finite-element modelling. This produced curvature changes. By fixing not only the TM ring but also the manubrium, and by applying pressures in the range of -7 to $+7$ kPa, the TM was deformed uniformly into new geometries. These new geometries were then taken as initial geometries where the manubrium was free to move again and a load of 10 Pa was applied again. In this manner, the model displacements were investigated as function of geometrical properties. By using finite-element simulations for the geometry development, the inaccuracy and subjectivity of manual curvature segmentation was avoided.

Chapter 4

Results

This chapter presents the results obtained from the 3-D reconstruction, the convergence study, the comparison between the two models with the chosen mesh resolution, and the displacement results from the geometrical sensitivity analysis.

4.1 Geometry

The resulting 3-D model for the 1-day-old left ear is presented in figure 4.1 at different orientations with visible mesh lines. As mentioned in chapter 4, the TM, pars flaccida, pars tensa, malleus, incus, AML and PIL were reconstructed from the CT scans. The TM geometry has an asymmetric shape. The tops of the malleus and incus heads look unfinished because of the limited number of slices. Also, the incus tip has a sharp form in the the 1-day-old middle ear, whereas the 22-day-old incus has a rounded tip. In contrast to the 22-day-old model, the manubrium is straight rather than curved. Furthermore, the posterior incudal ligaments differ in shape and are larger in the 1-day-old model.

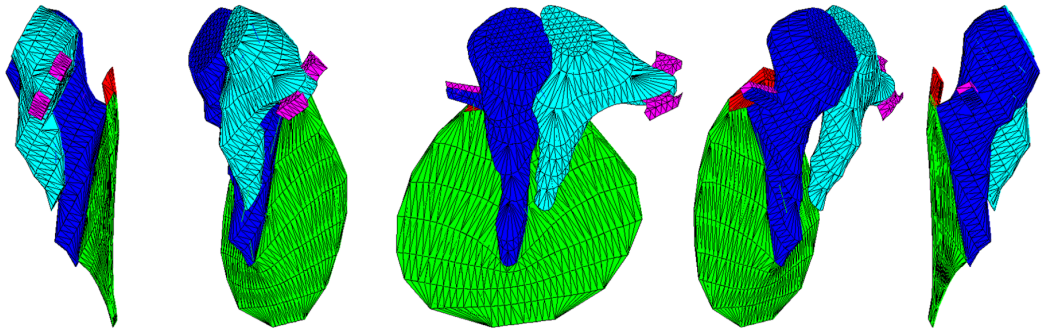

Figure 4.1: 1-day-old 3-D model with mesh lines comprising the tympanic membrane, pars tensa (green), pars flaccida (red), malleus (blue), incus (cyan) and ligaments (pink). The model is presented from five different angles.

Figure 4.2 depicts the 22-day-old model at similar angles. In comparison, the 22-day-old TM geometry looks slightly more circular and the malleus and incus heads look more rounded than to the 1-day-old model.

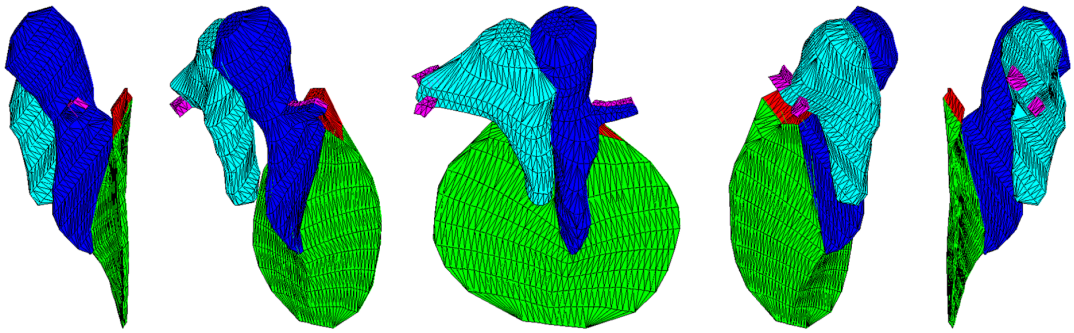

Figure 4.2: 22-day-old 3-D model with mesh lines comprising the tympanic membrane, pars tensa (green), pars flaccida (red), malleus (blue), incus (cyan) and ligaments (pink). The model is presented from five similar to those in 4.1 angles.

The TM of the 1-day-old model is based on segmentation lines in nine CT images, whereas the 22-day-old model is based on segmentation lines in eleven CT images. This leads to more nodes and a bigger size.

4.2 Convergence

The convergence study was performed with quadratic elements for both the 1-day-old model and the 22-day-old model. Both TM models were generated with the same five mesh xy-resolution values, which resulted in ten TM models. The TM ring was clamped while a load of 10 Pa was applied on the lateral side of the TM in each model. The initial mesh resolution xy-res=0 is based only on segmented nodes and contained 1240 and 1391 nodes for the 1-day-old and 22-day-old models, respectively, corresponding to 654 and 714 elements. The numbers of nodes of the models with higher mesh xy-resolutions increased as presented in figure 4.3. Since the 22-day-old model has two more slices in its segmentation, there is a difference in the number of nodes and elements as seen in the plot.

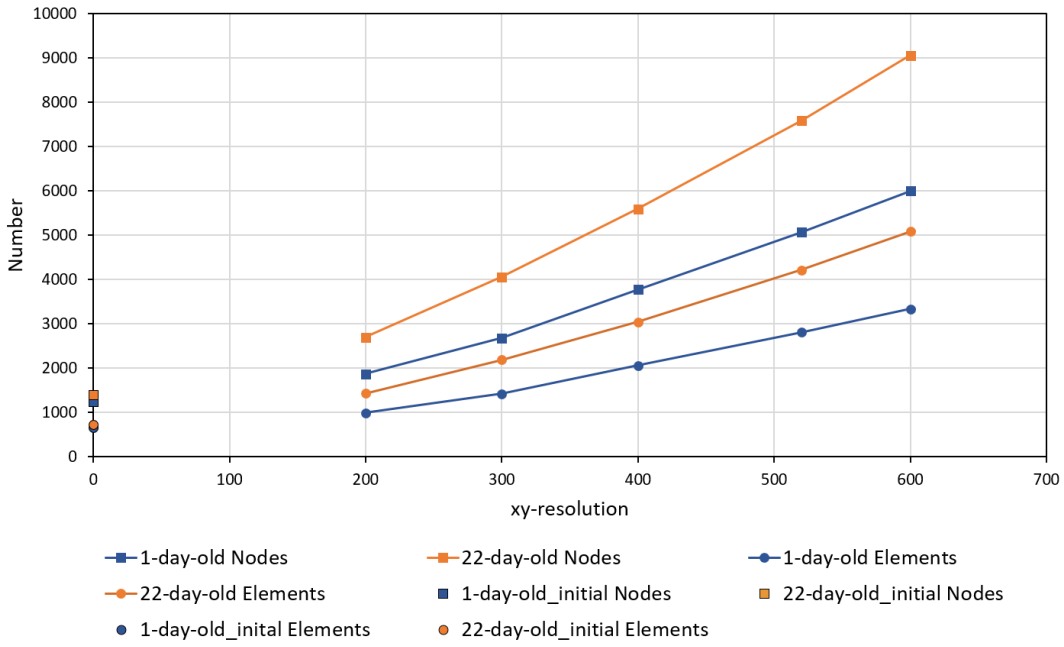

Figure 4.3: Numbers of nodes and elements for the TM models with different mesh resolutions for both ages. Five models with increasing xy-resolutions from 200 to 600 were generated by using the setting in Fie.

For the initial number of nodes without mesh refinement, the 1-day-old and 22-day-old models had displacements of 0.88 μm and 1.25 μm, respectively. The

resulting maximum TM displacements for each xy-resolution of the meshes are presented in figure 4.4.

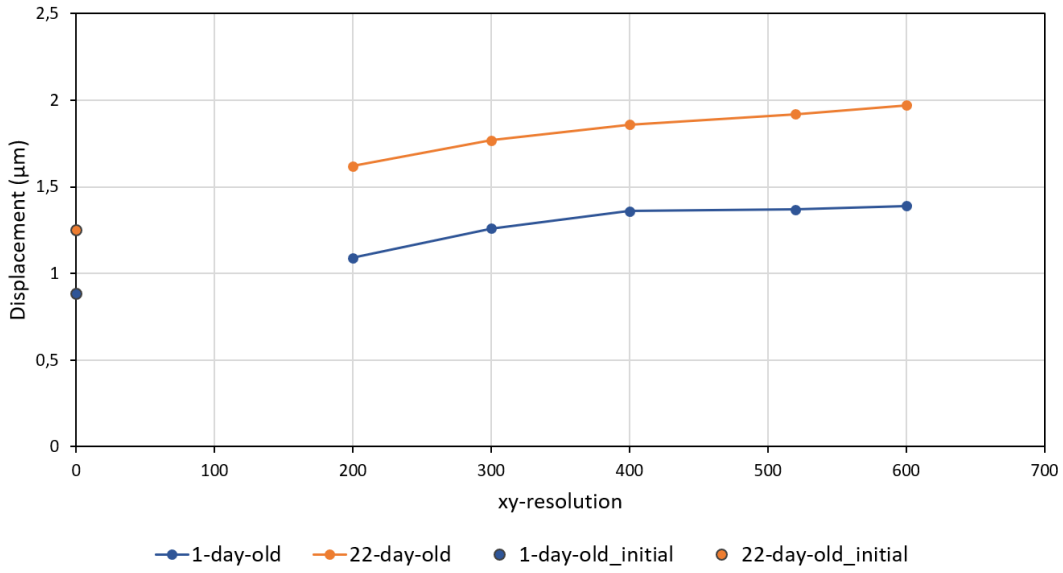

Figure 4.4: Results of convergence study for both TM models generated with different xy-resolutions of the mesh. The resulting maximum displacement is plotted for each mesh resolution.

As depicted, the results show a continuous increase in displacement with increasing mesh resolution. The 1-day-old model shows a plateau, while the 22-day-old model still shows an increasing displacement at xy-res=600. Simulations were also attempted at a mesh resolution of xy-res=700, which resulted in solution errors for both models. This might have been because of numerical problems due to the very fine mesh.

Based on these TM maximum displacement results, there is an advantage in using a higher mesh resolution than the initial mesh setting xy-res=0. As mentioned before, xy-res=0 means that the model is only based on the manually segmented nodes without refinement and redivision of segmentation lines. Table 4.1 presents a comparison of numbers of nodes and elements, displacements, and improvements between the initial state of the geometry with only segmented nodes and the models with higher mesh resolutions.

Table 4.1: Results of the convergence study listing the numbers of nodes and elements, maximum displacments (load = 10 Pa) and the displacement changes for the generated models with different mesh resolutions compared to the inital segmented model.

Model	**Initial state**	**xy200**	**xy300**	**xy400**	**xy520**	**xy600**
	Numbers of nodes					
1-day-old	1240	1869	2683	3777	5066	6003
22-day-old	1391	2700	4061	5593	7583	9060
	Numbers of elements					
1-day-old	654	991	1423	2057	2806	3340
22-day-old	714	1430	2187	3045	4213	5082
	Displacement (μm)					
1-day-old	0.88	1.09	1.26	1.36	1.37	1.39
22-day-old	1.25	1.62	1.77	1.86	1.92	1.97
	Displacement change compared to previous mesh resolution (%)					
1-day-old	-	23.4	15.6	7.9	0.7	1.5
22-day-old	-	29.6	9.3	5.1	3.2	2.6

As a trade-off, a mesh resolution was chosen that results in a high displacement accuracy without great computational expense. Therefore, the meshes with an xy-resolution setting of 400 was taken for both models for further simulations.

A comparison of the initial segmented TM and the TM with an xy-resolution of 400 is presented for both ages in figure 4.5 using 3-D visualizations with (1) visible mesh lines and (2) wire-frame style.

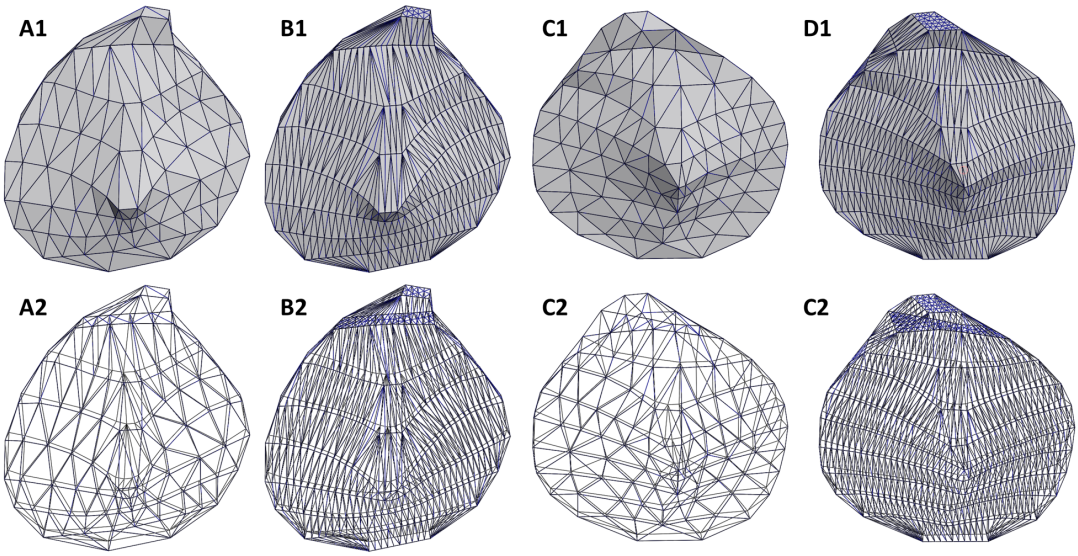

Figure 4.5: Medial views of 1-day-old and 22-day-old TM models, with the initial segmented mesh (A and C) and the mesh with the chosen xy-resolution of 400 (B and D). (1) 3-D models with visible mesh lines, and (2) 3-D models in wire-frame style.

In figure 4.6, another perspective illustrates the differences in 3-D shape and curvature. Especially for the 1-day-old model, an xy-resolution of 400, and thus a higher number of nodes and elements, shows a smoother curvature.

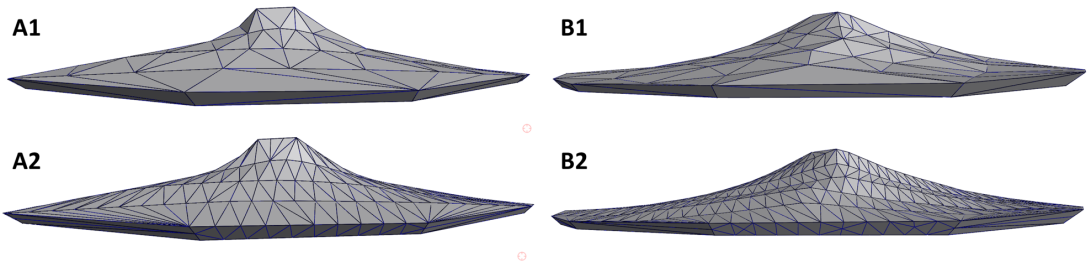

Figure 4.6: Presentation of the TM models at both ages (A=1-day-old and B=22-day-old) and both initial (1) and xy-400 (2) mesh resolutions.

A change in the xy-resolution will lead to slight changes in the 3-D shape. The goal is to use a mesh that is fine enough to achieve accurate results without requiring excessive computational time by having enough nodes specifying the desired shape.

4.3 Comparison of two different ages

For the comparison of the two middle-ear models at different ages, specific nodes were chosen for the displacement examination. Specifically, a node at the malleus tip (umbo) and a node at the incus tip were chosen for both models (figure 4.7). In order to evaluate the maximum TM displacement, the maximum value of the displayed scale bar was used. In the case of a second maximum peak on the TM, the displacement of the node closest to that local maximum was used.

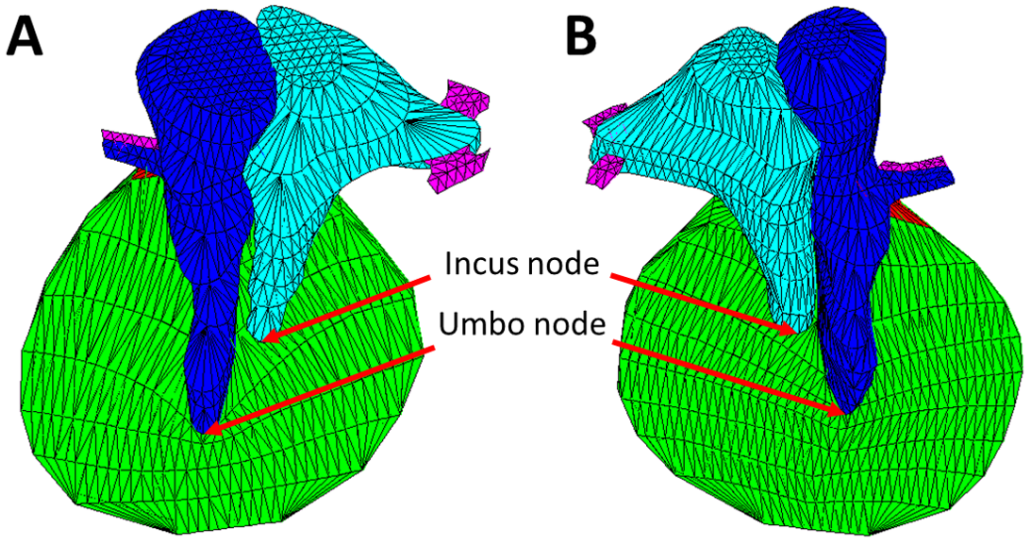

Figure 4.7: 3-D visualization of the middle-ear models at 1 day old (A) and at 22 days old (B) for xy-resolution=400. Both models include the same parts: TM (pars flaccida (red) and pars tensa (green)), malleus (blue), incus (cyan) and ligaments (pink). The red arrows point to the selected nodes for the incus and umbo that were examined in terms of displacement.

The resulting displacement behaviour is depicted in figure 4.8 as displayed in post view with a colour map showing the maximum displacement in white and the minimum displacement in black. The results in figure 4.9 were taken from PostView by selecting the specific nodes for the umbo and incus (see figure 4.7). The maximum TM displacements were obtained directly from the maximum values of the scale bars.

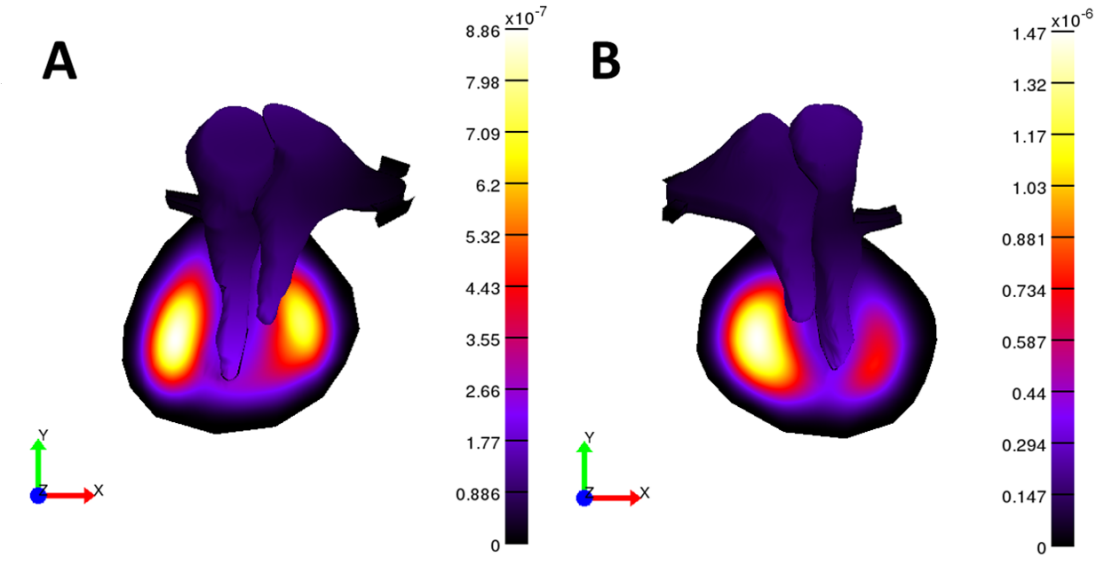

Figure 4.8: 1-day-old (A) and 22-day-old (B) simulation results as displayed in PostView. The colour map highlights the maximum displacement in white and the minimum displacement in black with a scale bar on the right side of each model with specific values given in meters. The spatial orientation is given by the axes in the left bottom corner of each panel.

The colour map highlights the locations of the peak displacements. The 1-day-old model shows two peaks on the TM, anterior and posterior to the manubrium with a greater magnitude on the anterior side. In comparison, the 22-day-old model also shows local maxima on the anterior and posterior sides of the TM, but with a larger difference in magnitude and with the greater magnitude located on the posterior side. Specific displacement values for incus tip, malleus tip, TM anterior and posterior for each model are compared in figure 4.9.

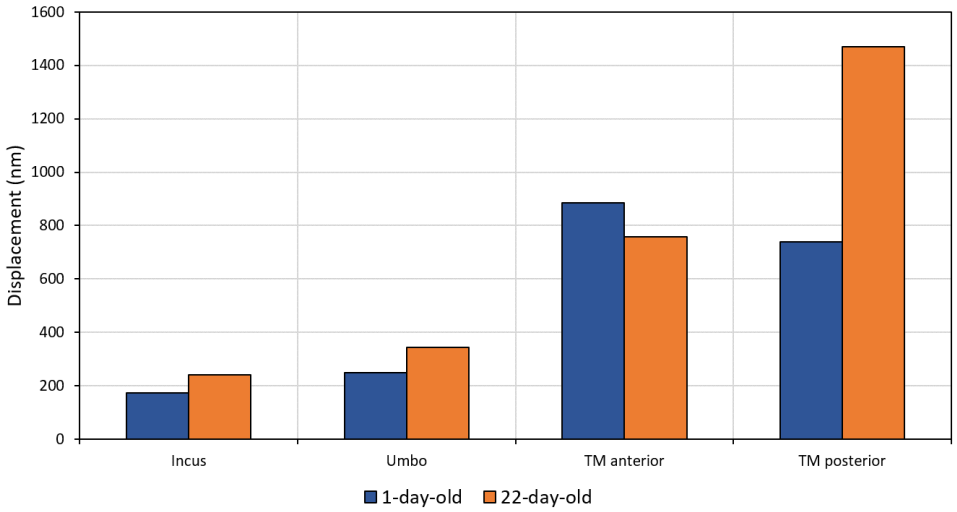

Figure 4.9: Displacement comparison of specific nodes at the incus tip, the malleus tip (umbo) and the TM with its local maxima on the anterior and posterior sides.

The 22-day-old model shows displacements that are larger by 39 % , 38 % and 99 % for the incus, umbo and posterior TM, respectively, but 14 % smaller for the anterior TM.

4.4 Sensitivity analysis

To investigate the effects of TM geometry on the displacement magnitude and behaviour, different curvatures based on the segmented geometry of the 1-day-old model were generated. More specifically, 11 different geometries were generated by applying five large positive loads and six large negative loads on the initial geometry. These loads were used purely to create new geometries, not to simulate actual mechanical behaviour. The resulting deformations were taken as initial geometries for new simulations with the same simulation parameters as the original model. To compare the displacement values, the same specific nodes as in section 4.3 were manually selected and examined for the malleus tip and the incus tip in PostView (figure 4.10). In case of the TM, the maximum displacement was examined again by the values obtained from the scale bars (figure 4.11). Additionally, the displacement values of the 22-day-old incus, umbo and TM posterior were added to the plot for comparison.

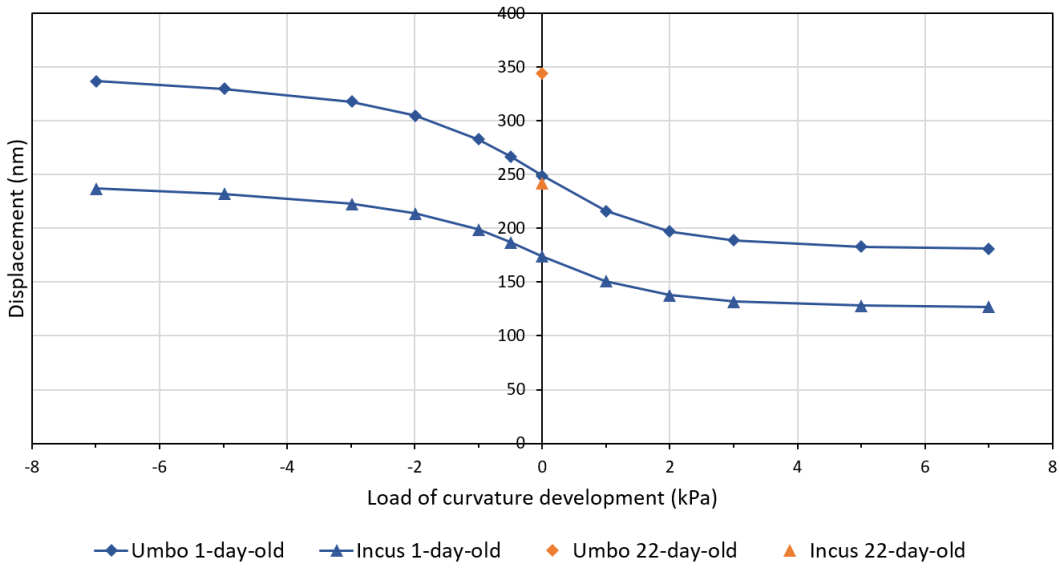

Figure 4.10: Displacement results for the eleven generated geometries and their baseline at specific incus and umbo nodes. The x-axis represents the loads that were applied to the baseline (initial segmented model) to achieve the deformation that led to the resulting geometry. The baseline is at 0 kPa since no pressure was applied to get the geometry. All results are obtained by a load (static pressure) of 10 Pa on the lateral TM side with fixed TM ring and ligament ends. In addition, the 22-day-old incus and umbo displacements are added for comparison.

It can be seen that all geometries resulting from negative applied loads resulted in higher umbo and incus displacements and all geometries resulting from positive applied loads led to lower umbo and incus displacements compared to the baseline (0 kPa). Furthermore, the higher the negatively applied load the higher was the ossicular displacement. The steepest slopes are at 0 kPa, and the curves plateau at high negative and positive applied pressures.

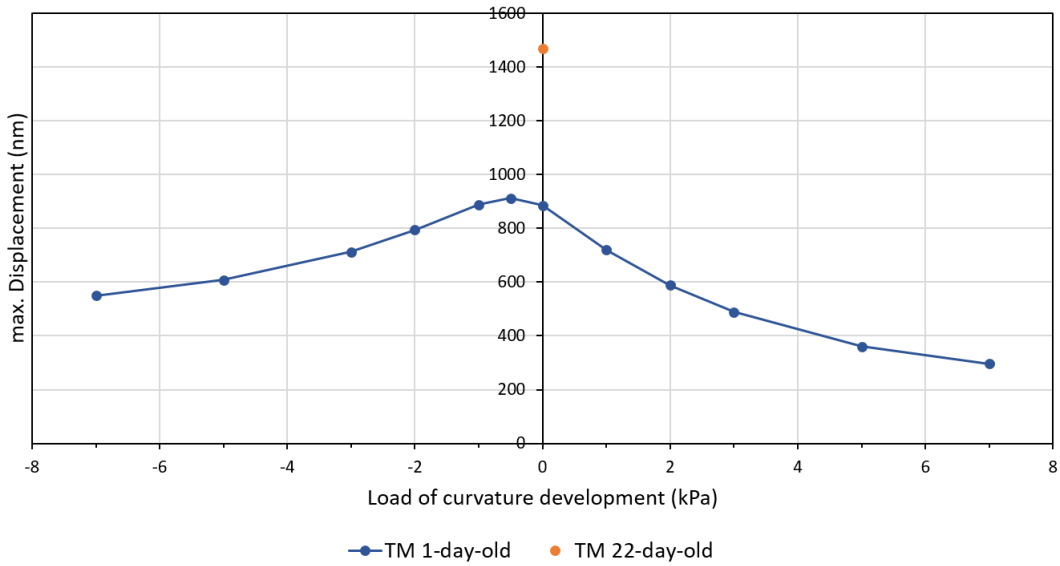

Figure 4.11: Maximum displacement results for the eleven generated geometries and their baseline at the TM. The x-axis represents the loads that were applied to the baseline (initial segmented model) to achieve the deformation that led to the resulting geometry. The baseline is at 0 kPa since no pressure was applied to get the geometry. All results are obtained by a load (static pressure) of 10 Pa on the lateral TM side with fixed TM ring and ligament ends. In addition, the 22-day-old maximum TM displacements is added for comparison.

The TM maximum displacement results are presented in the same way in figure 4.11. The maximum TM displacement is obtained with the geometry generated with -500 Pa applied to the baseline model with a slightly higher displacement than the value from the baseline model. Apart from the -500 Pa and -1000 Pa models, both geometry series, generated from negative and positive applied loads, show decreased TM displacement compared to the baseline model, with the geometry series from the positive applied loads showing the lowest TM displacement values.

Chapter 5

Discussion

5.1 CT scan quality

Since the 3-D model can only be as good as the segmentation and the segmentation only as accurate as the CT scan resolution and quality allow, the image quality needs to be discussed. As both imaging settings and properties such as slice thickness, scan option (helical), reconstruction diameter, exposure time, image focus (mastoids) and imaging device are the same for our two cases, the differences are in patient-dependent factors. As highlighted in section 3.3.3, the contrast was worse in the 1-day-old images than in the 22-day-old images, apparently due to possible amniotic fluid or mesenchyme in the middle-ear cavity, leading to an increased level of uncertainty in the segmentation and thus to possible decreased accuracy of the 3-D model reconstruction.

5.2 Convergence

The results in section 4.2 showed that the chosen xy-res=400 led to a displacement increase of 54 % for the 1-day-old model and 49 % for the 22-day-old model when compared to the initial segmented models with only segmented nodes (xy-res=0). To evaluate not only the maximum displacement magnitudes from the TM models as presented in section 4.2 but also displacement pattern differences, the whole models were analysed once with xy-res=0 as initially segmented and once with the chosen xy-res=400. Figure 5.1 depicts the 1-day-old model with clamped TM

ring and ligament ends with a load of 10 Pa, with (A) the number of nodes as segmented (6217) and (B) the increased number of nodes (10871). One can see that not only the maximum displacement magnitude in the anterior region of the TM increased but also that the posterior vibration region became more clearly separated from the anterior region.

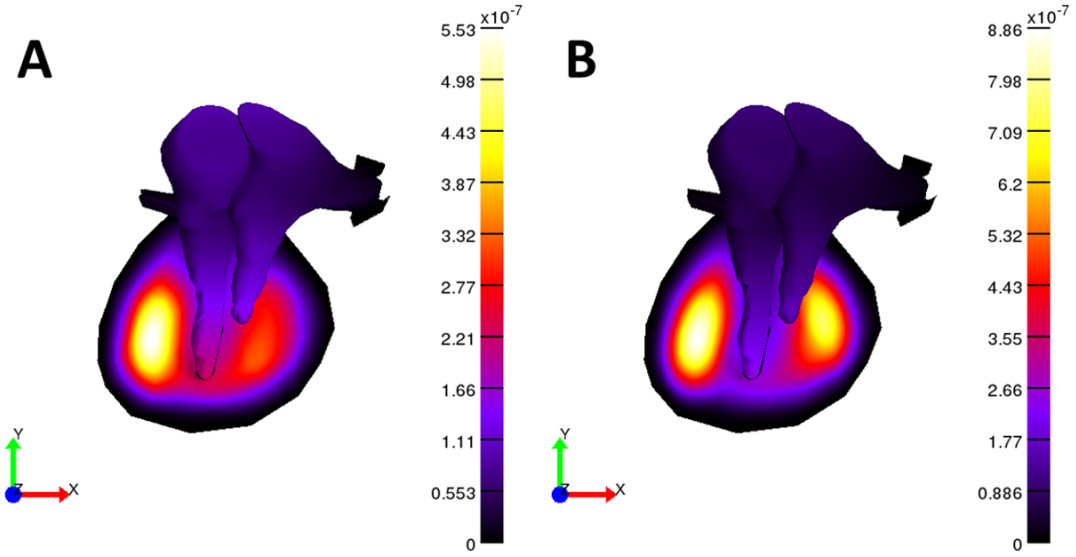

Figure 5.1: Presentation of the whole 1-day-old model with clamped TM ring and ligament ends and applied load of 10 Pa on the TM with (A) the number of nodes as initially segmented and (B) an increased number of nodes with the chosen xy-resolution of 400 from the convergence study. The colour map highlights the displacement behaviour with maximum displacement being white and minimum displacement being black, with corresponding scale bars on the right with specific values given in meters.

In comparison, the whole 22-day-old model is presented in figure 5.2 with the same boundary conditions and both mesh resolutions, namely the initial segmented state with only segmented nodes (xy-res=0) and the refined xy-res=400.

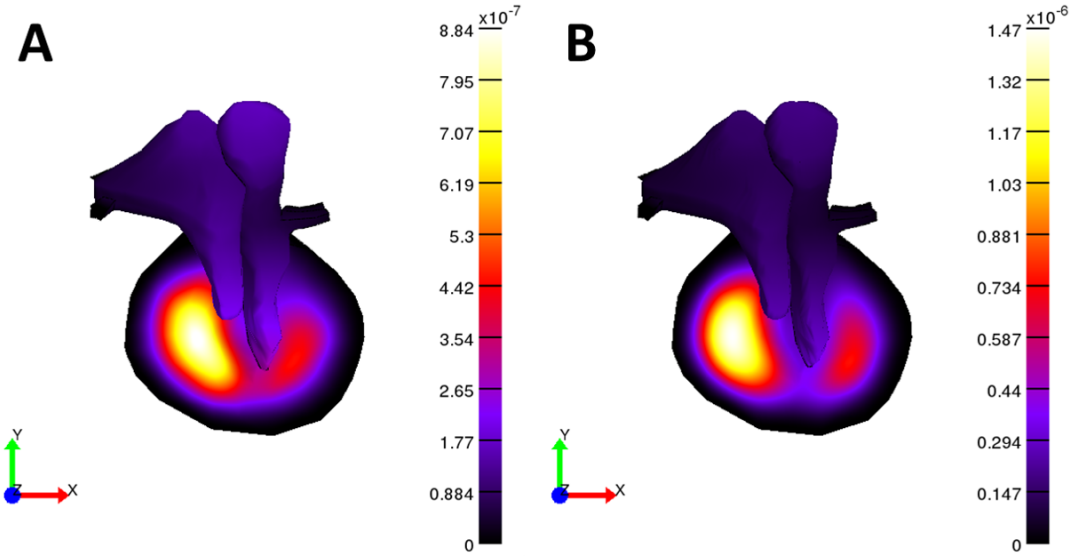

Figure 5.2: Presentation of the whole 22-day-old model with clamped TM ring and ligament ends and applied load of 10 Pa on the TM with (A) the number of nodes as initially segmented and (B) an increased number of nodes with the chosen xy-resolution of 400 from the convergence study. The colour map highlights the displacement behaviour with maximum displacement being white and minimum displacement being black, with corresponding scale bars on the right with specific values given in meters.

Here also, the anterior and posterior vibration regions became clearly more separated. These observations are a result of the increased number of nodes that describe the geometry in a more refined way.

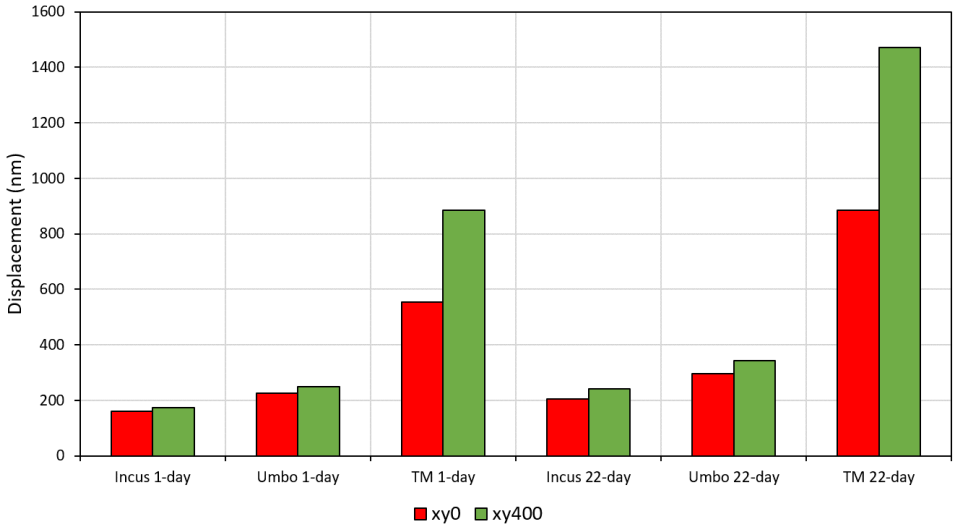

Figure 5.3: Displacement comparison for the initial segmented model (xy0) and the xy-mesh refined model (xy400) at both ages. Specific nodes at the incus tip, malleus tip (umbo) and TM displacement maximum were examined.

Although the maximum TM displacement increased by 60 % for the 1-day-old and 66 % for the 22-day-old, the incus and umbo displacements only increased by 9 % and 10 % for the 1-day-old and 18 % and 16 % for the 22-day-old.

Due to software limitations, the convergence study involved mesh refinement only in the *xy* direction and only for the TM. The mesh refinement of the ligaments could have major effects on the model behaviour, but it was not tested separately. Furthermore, with only one layer of elements in depth for the TM, the model might be stiffer than it should be. The conversion to quadratic elements increased the accuracy of the model but, without a mesh refinement in all directions, limitations in accuracy need to be considered. Additionally, the conversion method from linear to quadratic elements was newly implemented and still needs to be verified by a comparison of the results with different FEM software.

5.3 Comparison of two ages

As presented in the results section, the 22-day-old model had overall higher displacements than the 1-day-old model at the incus, malleus and TM . This might

have been due to the previously mentioned segmentation differences such as better contrast and identifiability of certain structures. The level of uncertainty might have led to a suboptimal geometry in the 1-day-old 3-D reconstruction.
Another reason could be the size differences of the ossicles. Since the ossicles have been said to grow after birth [18], the 22-day-old ossicles might be expected to be larger. Fad was used to measure the approximate size of the ossicles and the TM by manually selecting two nodes in the 3-D model (table 5.1). The 22-day-old incus and manubrium lengths were smaller but the other 22-day-old model parts were found to be somewhat larger. The curved shape of the 22-day-old manubrium was not considered in the measurement. Given the low resolution of the CT images, these measurement are very approximate.

Table 5.1: Approximate sizes of the ossicles and the TM as measured by Fad.

	1-day-old	**22-day-old**
TM width (mm)	7.8	8.8
TM length (mm)	8.4	8.8
Malleus length (mm)	8.6	9.2
Incus length (mm)	6.8	6.7
Manubrium length (mm)	5.4	4.9

Although the slice thickness and other imaging settings were the same, differences are also visible in the numbers of images that contain the TM, malleus and incus. The TM, malleus and incus are visible in the 1-day-old scan in 9, 11 and 8 slices, respectively. In contrast, these parts are visible in the 22-day-old model in 11, 15 and 10 slices, respectively. This could be due to different head orientations during scanning. It might be also related to differences in image contrast.
Furthermore, the differences in the TM displacement patterns might be traced to geometrical differences. Figure 4.6 shows that the curvature of the 22-day-old TM is spread over the whole TM span, while the 1-day-old TM curvature is mainly concentrated in the region close to the manubrium. The rest of the TM looks rather straight for the 1-day-old TM. These geometrical differences presumably affect the TM displacement magnitudes and patterns, and the transmission

of vibrations to the malleus and incus. However, these apparent differences in curvature are not reliable due to uncertainty in the segmentation.

To the best of our knowledge experimental direct measurements are available for the TM displacement of newborns. However, Motallebzadeh et al. reported results with the 22-day-old model, with the same boundary conditions and an applied sound stimulus of 0.2 Pa and compared the simulation results with clinical admittance measurements [38]. The frequency of their input pressure varied from 250 Hz to 2000 Hz. At 250 Hz, using Code_Aster as the FE solver, they observed a maximum TM displacement of 36 nm. The present 22-day-old model with static input pressure of 0.2 Pa results in a maximum TM displacement of 29 nm. This is close to the 36 nm obtained by Motallebzadeh et al. with their model, and their model approximately matched clinical admittance measurements, thus providing a validation of the present model.

5.4 Sensitivity analysis

To develop an understanding of how the developed curvatures led to the presented results of section 4.4, figure 5.4 depicts three curvatures in inferior views of the initial segmented 1-day-old model as baseline (A), of the model generated with -7 kPa applied pressure on the baseline (B) and of the model developed with $+7$ kPa applied pressure on the baseline (C). A is seen to be mildly concave, B is more concave, and C is convex. Matching these findings to the results presented in figures 4.10 and 4.11, one can conclude first that a rather concave curvature is favourable for displacement transmission and thus for ossicular movement. This is proportional to the degree of concavity, which is increased with the increase of negative pressure and results in an increase in mallear and incudal movement. Second, the convex curvature is the least favourable for osscicular and TM movement. The convexity might make the TM stiffer and therefore decrease the displacement and leads to a plateau. Lastly, the mildly concave TM curvature leads to the highest TM displacement but is not optimal for ossicular transmission. The presented results show that the geometry of the TM, and especially the curvature, has a big impact on the displacement behaviour. Not only

the TM displacement magnitude but also the ossicular transmission are crucially dependent on the TM geometry.

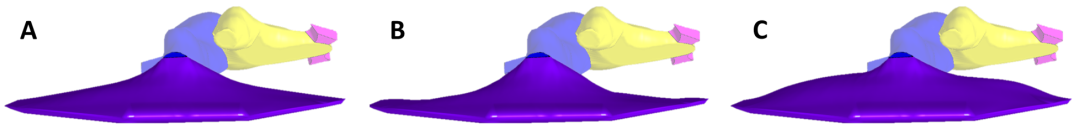

Figure 5.4: Curvature comparison showing inferior views of the initial segmented 1-day-old TM (baseline)(A), of the baseline TM deformed by an applied load of −7 kPa (B) and of the baseline TM deformed by an applied load of +7 kPa (C).

To identify displacement patterns for favourable behaviours, figure 5.5 shows the displacement patterns corresponding to the generated curvatures for each simulated model. Boundary conditions (fixed TM ring and ligament ends and 10 Pa pressure applied on the lateral TM side) were the same as for the baseline model. Additionally, the *xz* plane perspective of each curvature is depicted above each displacement pattern. The pressures that were used to generate the TM shapes are indicated in the left bottom corner of each panel.
The colour patterns illustrate how, for both negative and positive pressures, the area of maximum displacement (white) increases on the TM for increasing pressure of curvature development. The area participation in displacement of the TM increases although the TM maximum displacement magnitude decreases. The greater amount of TM area with nearly maximum displacement leads in the concave models to a greater ossicular movement. However, the same is happening for the convex models and the ossicular movement decreases. The TM displacement pattern and the amount of participating TM area are not good indicators for good displacement transmission to the ossicles.

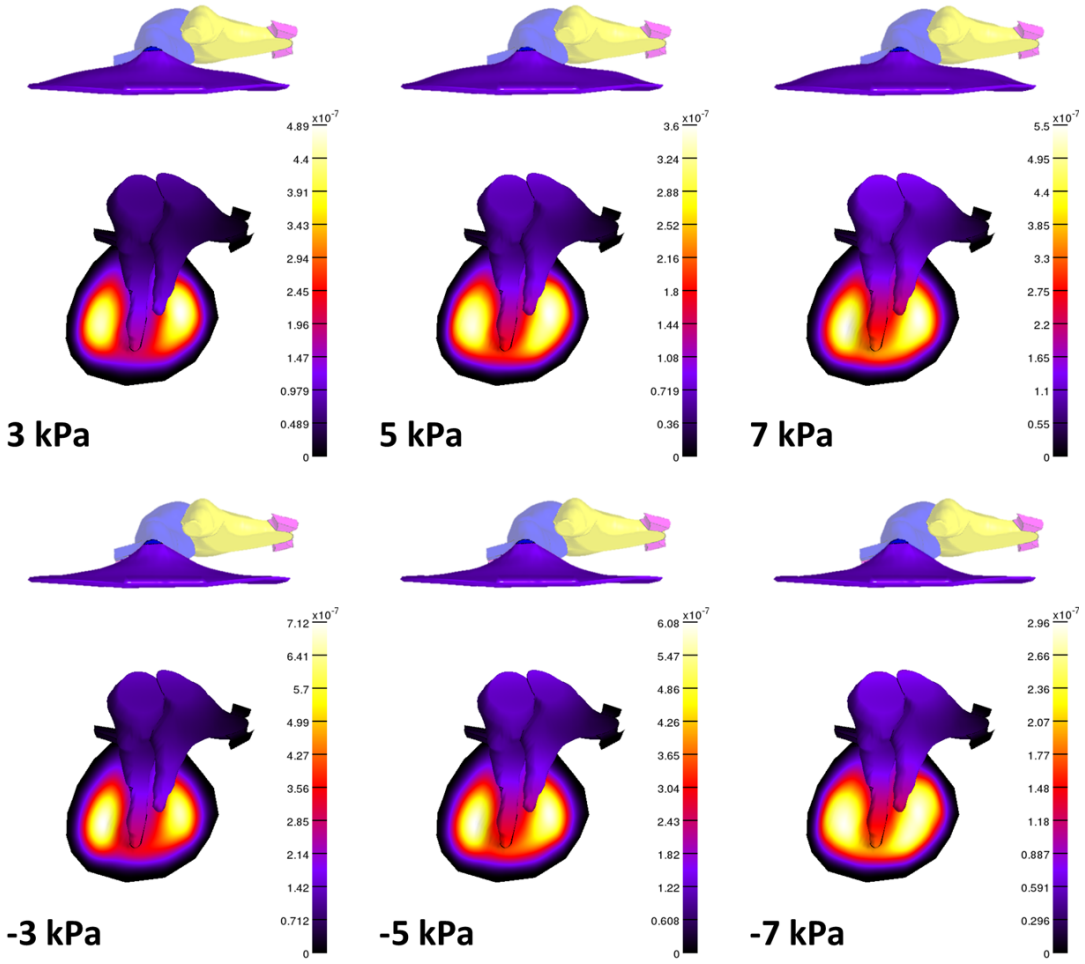

Figure 5.5: Displacement patterns for the developed geometries resulting from the large positive and negative applied load on initially segmented model (xy-resolution 400). The curvature is presented as an xz-projection above each displacement pattern. The load magnitude of geometry development is denoted in the left bottom corners. The maximum displacement, resulting from a pressure of 10 Pa applied on the lateral TM side, is depicted in white and the minimum displacement in black according to the colour bars on the right, with specific displacement values given in meters.

5.5 Limitations

The main limitations of the project are the following:

- **Anatomical simplifications**

  Simplifications like a fused malleus and incus without incudomallear joint,

and no stapes or incudostapedial joint, have been made. The TM ring is simply fixed.

- **CT resolution**
  Difficulties in recognizing non-bony and small structures, like the TM, stapes and anterior process of malleus and its ligament, always led to a level of uncertainty.

- **Mesh refinement**
  The mesh refinement was not performed in all directions and the TM mesh consists of only one layer of elements. The fact that the mesh refinement was only performed in the xy direction led to more elongated thin triangular elements and thus possible numerical errors due to high element aspect ratios.

- **Conversion to quadratic elements**
  The element conversion method from linear to quadratic was not thoroughly verified but appeared to be correct.

- **Low-frequency simulation**
  Sine only a static input pressure was simulated, the results are only relevant to low frequencies. Therefore, the model analysis needs to be extended to higher frequencies where inertial and damping effects become more significant.

Chapter 6

Conclusion

6.1 Conclusion

In the comparison of the two ages, different displacement behaviours were observed. Both models were analysed under the same conditions such, with the same element conversion method, the same mesh-refinement parameters and method and the same boundary conditions. The only differences were in the image segmentation and patient-specific geometry. The CT scan quality for the 1-day-old model was found to be worse than that for the 22-day-old model. This might have been related to the age difference since 1-day-old infants often still have amniotic fluid and/or mesenchyme inside the middle-ear cavity. Good CT scan quality is crucial for the 3-D reconstruction since uncertainty in the segmentation leads to further error in the simulated behaviour.

The simulations were run with linear elements first before the conversion method to quadratic elements was implemented. The conversion from linear to quadratic elements had dramatic effects. It is always recommended to at least consider the use of higher-order elements.

In contrast to sensitivity analysis for the material properties, geometrical sensitivity analysis is more difficult to perform and has thus been done less often. Using the FEM method to generate new geometries by applying large pressures to a baseline model in order to obtain uniform deformations was shown to be a

good alternative to doing multiple image segmentations.
The sensitivity analysis with different generated geometries of the 1-day-old TM demonstrated the importance and impact of TM geometry and curvature. Furthermore, it showed that specific curvatures can be favourable for higher TM displacement or higher ossicular displacement.

6.2 Future work

Verification of the results with another FEM solver such as Code_Aster would be a valuable step.

Since material properties such as the Youngs's modulus are not well known for the newborn TM, further investigations like a sensitivity analysis of the material properties would clarify their influence on the results.

Another useful analysis would be an investigation of the influence of the ligaments and thus of the rotational axis on the results by performing a separate convergence study and a material-property sensitivity analysis for the ligaments.

Due to the poor CT-scan resolution, anatomical structures such as the incudomallar joint, incudostapedial joint and stapes were not included in the model. Micro-CT images, histological sections or other imaging with higher resolution would allow us to improve the model accuracy.

Finally, this work presented investigations on the newborn middle ear in the linear range with small pressures and with a static input without inertial and damping effects. Non-linear and time-dependent simulations are required to develop a better understanding of realistic conditions.

List of Figures

List of Tables

Bibliography

[1] Cynthia C Morton and Walter E Nance. Newborn hearing screening-a silent revolution. *New England Journal of Medicine*, 354(20):2151–2164, 2006.

[2] Joint Committee on Infant Hearing et al. Year 2007 position statement: Principles and guidelines for early hearing detection and intervention programs. *Pediatrics*, 120(4):898–921, 2007.

[3] Anna MH Korver, Richard JH Smith, Guy Van Camp, Mark R Schleiss, Maria AK Bitner-Glindzicz, Lawrence R Lustig, Shin-ichi Usami, and An N Boudewyns. Congenital hearing loss. *Nature Reviews Disease Primers*, 3: 16094, 2017.

[4] Michael Schünke, Erik Schulte, and Udo Schumacher. *PROMETHEUS Lern-Atlas der Anatomie: Kopf, Hals und Neuroanatomie, 2., Auflage.* Thieme, Stuttgart, 2009.

[5] Peter Cull. *The sourcebook of medical illustration: Over 900 anatomical, medical, and scientific illustrations available for general re-use and adaptation free of normal copyright restrictions.* Parthenon Publishing, 1989.

[6] Dwight W Batteau. The role of the pinna in human localization. *Proceedings of the Royal Society of London. Series B. Biological Sciences*, 168(1011):158–180, 1967.

[7] Richard L Drake and Lars Bräuer. *Atlas der Anatomie.* Elsevier, Urban&FischerVerlag, 2009.

[8] Barry Joseph Anson and James A Donaldson. *Surgical anatomy of the temporal bone*, volume 31. Saunders Philadelphia, 1981.

[9] DJ Lim. Human tympanic membrane: An ultrastructural observation. *Acta oto-laryngologica*, 70(3):176–186, 1970.

[10] Liesbeth C Kuypers, Willem F Decraemer, and Joris JJ Dirckx. Thickness distribution of fresh and preserved human eardrums measured with confocal microscopy. *Otology & Neurotology*, 27(2):256–264, 2006.

[11] GabrieleTraviglia. *External ear: Tympanic membrane*, 2016 (accessed January, 2020). URL `https://www.cram.com/flashcards/anatomy-and-physiology-of-the-hearing-system-7018335`.

[12] Carlos B Ruah, Patricia A Schachern, Daniel Zelterman, Michael M Paparella, and Tae H Yoon. Age-related morphologic changes in the human tympanic membrane: A light and electron microscopic study. *Archives of Otolaryngology–Head & Neck Surgery*, 117(6):627–634, 1991.

[13] OW Henson and Miriam M Henson. The tympanic membrane: Highly developed smooth muscle arrays in the annulus fibrosus of mustached bats. *Journal of the Association for Research in Otolaryngology*, 1(1):25–32, 2000.

[14] MM Henson, VJ Madden, Helge Rask-Andersen, and OW Henson Jr. Smooth muscle in the annulus fibrosus of the tympanic membrane in bats, rodents, insectivores, and humans. *Hearing research*, 200(1-2):29–37, 2005.

[15] Stefan LR Gea, Willem F Decraemer, Robert WJ Funnell, Joris JJ Dirckx, and Hannes Maier. Tympanic membrane boundary deformations derived from static displacements observed with computerized tomography in human and gerbil. *Journal of the Association for Research in Otolaryngology*, 11 (1):1–17, 2010.

[16] George Noussios, Pantelis Chouridis, Lazaros Kostretzis, and Konstantinos Natsis. Morphological and morphometrical study of the human ossicular chain: A review of the literature and a meta-analysis of experience over 50 years. *Journal of clinical medicine research*, 8(2):76, 2016.

[17] B Arensburg, M Harell, and H Nathan. The human middle ear ossicles:

Morphometry, and taxonomic implications. *Journal of Human Evolution*, 10(2):199–205, 1981.

[18] J Olszewski. Zur morphometrie der gehörknöchelchen beim menschen im rahmen der entwicklung. *Anatomischer Anzeiger*, 171(3):187–191, 1990.

[19] Tomoko Yokoyama, Yukiko Iino, Keiko Kakizaki, and Yoshihiko Murakami. Human temporal bone study on the postnatal ossification process of auditory ossicles. *The Laryngoscope*, 109(6):927–930, 1999.

[20] Marc Giacone. *Auditory ossicles*, 2017 (accessed January, 2020). URL `https://en.wikipedia.org/wiki/Incudostapedial_joint?`

[21] MD Graham, Carl Reams, and Rodney Perkins. Human tympanic membrane-malleus attachment preliminary study. *Annals of Otology, Rhinology & Laryngology*, 87(3):426–431, 1978.

[22] Aage R Møller. The acoustic middle ear muscle reflex. In *Auditory system*, pages 519–548. Springer, 1974.

[23] Xuan Wang. *Finite-element Modelling of the Human Middle Ear Based on X-ray Micro-computed Tomography and Doppler Optical Coherence Tomography in the Same Ear*. PhD thesis, McGill University Libraries, 2019.

[24] Takuji Koike, Hiroshi Wada, and Toshimitsu Kobayashi. Modeling of the human middle ear using the finite-element method. *The Journal of the Acoustical Society of America*, 111(3):1306–1317, 2002.

[25] JJ Guinan Jr and WT Peake. Middle-ear characteristics of anesthetized cats. *The Journal of the Acoustical Society of America*, 41(5):1237–1261, 1967.

[26] William A Yost, Donald W Nielsen, and Glenis R Long. Fundamentals of hearing: An introduction, by william a. yost and donald w. nielsen, 1986.

[27] H von Helmholtz. Die mechanik der gehoerknoechelchen und des trommelfells. *Pflügers Archiv European Journal of Physiology*, 1(1):1–60, 1868.

[28] Juergen Tonndorf and Shyam M Khanna. The role of the tympanic membrane in middle ear transmission. *Annals of Otology, Rhinology & Laryngology*, 79(4):743–753, 1970.

[29] W Robert J Funnell. Low-frequency coupling between eardrum and manubrium in a finite-element model. *The Journal of the Acoustical Society of America*, 99(5):3036–3043, 1996.

[30] Robert D Cook et al. *Concepts and applications of finite element analysis*. John Wiley & Sons, 2007.

[31] William Robert John Funnell. *A theoretical study of eardrum vibrations using the finite-element method*. PhD thesis, McGill University, 1975.

[32] W Robert J Funnell and Charles A Laszlo. Modeling of the cat eardrum as a thin shell using the finite-element method. *The Journal of the Acoustical Society of America*, 63(5):1461–1467, 1978.

[33] W Robert J Funnell. On the undamped natural frequencies and mode shapes of a finite-element model of the cat eardrum. *The Journal of the Acoustical Society of America*, 73(5):1657–1661, 1983.

[34] W Robert J Funnell, Willem F Decraemer, and Shyam M Khanna. On the damped frequency response of a finite-element model of the cat eardrum. *The Journal of the Acoustical Society of America*, 81(6):1851–1859, 1987.

[35] Daniel De Greef, Felipe Pires, and Joris JJ Dirckx. Effects of model definitions and parameter values in finite element modeling of human middle ear mechanics. *Hearing research*, 344:195–206, 2017.

[36] Li Qi, Hengjin Liu, Justyn Lutfy, W Robert J Funnell, and Sam J Daniel. A nonlinear finite-element model of the newborn ear canal. *The Journal of the Acoustical Society of America*, 120(6):3789–3798, 2006.

[37] Li Qi, W Robert J Funnell, and Sam J Daniel. A nonlinear finite-element model of the newborn middle ear. *The Journal of the Acoustical Society of America*, 124(1):337–347, 2008.

[38] Hamid Motallebzadeh, Nima Maftoon, Jacob Pitaro, W Robert J Funnell, and Sam J Daniel. Finite-element modelling of the acoustic input admittance of the newborn ear canal and middle ear. *Journal of the Association for Research in Otolaryngology*, 18(1):25–48, 2017.

[39] Hamid Motallebzadeh, Nima Maftoon, Jacob Pitaro, W Robert J Funnell, and Sam J Daniel. Fluid-structure finite-element modelling and clinical measurement of the wideband acoustic input admittance of the newborn ear canal and middle ear. *Journal of the Association for Research in Otolaryngology*, 18(5):671–686, 2017.

[40] Li Qi. *Non-linear finite-element modelling of newborn ear canal and middle ear*. PhD thesis, McGill University, 2008.

[41] Hamid Motallebzadeh. *Finite-element models related to wideband tympanometry in newborns*. PhD thesis, McGill University, 2015.

[42] JJJ Dirckx and WF Decraemer. Effect of middle ear components on eardrum quasi-static deformation. *Hearing research*, 157(1-2):124–137, 2001.

[43] Clayton T McKee, Julie A Last, Paul Russell, and Christopher J Murphy. Indentation versus tensile measurements of young's modulus for soft biological tissues. *Tissue Engineering Part B: Reviews*, 17(3):155–164, 2011.

[44] Stephen C Cowin. *Bone mechanics handbook*. CRC press, 2001.

[45] W Robert J Funnell and Charles A Laszlo. A critical review of experimental observations on ear-drum structure and function. *Journal for Oto-Rhino-Laryngology, Head and Neck Surgery*, 44(4):181–205, 1982.

[46] WF Decraemer and WRJ Funnell. Anatomical and mechanical properties of the tympanic membrane. *Chronic Otitis Media. Pathogenesis-Oriented Therapeutic Management*, pages 51–84, 2008.

[47] Hiroshi Yamada, F Gaynor Evans, et al. Strength of biological materials. 1970.

[48] H Rollhäuser. Die zugfestigkeit der menschlichen haut. *Gegenbaurs Morph Jb*, 90:249–261, 1950.

[49] Joris AM Soons, Jef Aernouts, and Joris JJ Dirckx. Elasticity modulus of rabbit middle ear ossicles determined by a novel micro-indentation technique. *Hearing research*, 263(1-2):33–37, 2010.

[50] Bin Feng and Rong Z Gan. Lumped parametric model of the human ear for sound transmission. *Biomechanics and modeling in mechanobiology*, 3(1): 33–47, 2004.

Declaration of Authorship

I hereby declare that the thesis submitted is my own unaided work. All direct or indirect sources used are acknowledged as references. I am aware that the thesis in digital form can be examined for the use of unauthorized aid and in order to determine whether the thesis as a whole or parts incorporated in it may be deemed as plagiarism. For the comparison of my work with existing sources I agree that it shall be entered in a database where it shall also remain after examination, to enable comparison with future theses submitted. Further rights of reproduction and usage, however, are not granted here. This paper was not previously presented to another examination board and has not been published.

First and last name city, date and signature

Appendix A

Content of CD

- Master thesis documentation in PDF format
- PowerPoint presentation in PDF format